A&A 524, A99 (2010)
DOI: 10.1051/0004-6361/201014810

Astronomy & Astrophysics

Outburst OH maser activity in the envelopes of S Persei and VX Sagittarii⋆,⋆⋆

M. Szymczak[1], P. Wolak[1], E. Gérard[2], and A. M. S. Richards[3]

[1] Toruń Centre for Astronomy, Nicolaus Copernicus University, Gagarina 11, 87-100 Toruń, Poland
e-mail: msz@astro.uni.torun.pl
[2] GEPI, UMR 8111, Observatoire de Paris, 5 place J. Janssen, 92195 Meudon Cedex, France
[3] Jodrell Bank Centre for Astrophysics, School of Physics and Astronomy, University of Manchester, M13 9PL, UK

Received 16 April 2010 / Accepted 6 August 2010

ABSTRACT

Context. OH masers from the envelopes of M-type supergiants show a significant degree of polarization, implying magnetic fields of a few mG. Nothing is known about the temporal characteristics of the magnetic fields or how such changes may affect stellar mass loss.
Aims. We therefore observed two supergiant stars in order to quantify the long-term polarization behaviour of the maser emission.
Methods. Full-polarization spectra at 1612 and 1667 MHz were obtained with the Nançay radio telescope at intervals over periods of 4 and 6 years for S Per and VX Sgr, respectively.
Results. Time series of OH maser full polarization spectra are presented. Semiregular variations of the integrated flux densities generally follow the visual light curves as expected for radiative pumping cycles. For both sources the variability indices of individual features are higher at 1667 MHz than at 1612 MHz and their extreme values occur for the blue-shifted emission. The degrees of polarization at 1667 MHz show diverse behaviours usually uncorrelated with the total flux, whereas those at 1612 MHz are commonly stable on time scales of 4−6 yr. Several outbursts of the 1667 MHz emission on time scales of 0.5−2 yr were found in both targets. The bursting features are highly polarized and show drifts in velocity. Small changes of the degrees of polarization and smooth variations of position angle of linear polarization during the bursts were observed in S Per but they are more dramatic in VX Sgr.
Conclusions. The OH outbursts do not seem to have any direct link to stellar events, but seem to be localized in the wind.

Key words. masers – polarization – circumstellar matter – supergiants – stars: individual: S Per – stars: individual: VX Sgr

1. Introduction

Red supergiants (RSGs) of enormous luminosity $10^{5.5}$ $L_\odot$ and low effective temperature ∼3400–3600 K (Levesque et al. 2005) are likely in the latest phases of evolution as signposted by high mass loss rates of at least 10^{-4} $M_\odot$ yr^{-1} and violent maser activity (e.g. Richards et al. 1999; Schuster et al. 2006 and references therein). Their thick dust-gas envelopes usually hamper an accurate determination of the central star properties, but make them excellent targets for studies of the gas properties and magnetic fields at distances up to several hundred stellar radii where OH masers operate (e.g. Chapman & Cohen 1986; Richards et al. 1999).

RSGs' OH spectra of 30–50 km s^{-1} width are rich and diverse in polarized features when observed with a 0.1 km s^{-1} resolution (Cohen et al. 1987). The direction and strength of the magnetic field are directly measured from Zeeman splitting (Chapman & Cohen 1986; Szymczak & Cohen 1997) while its projection on the plane of the sky is inferred from linearly polarized features. At distances of OH maser formation (100–1400 AU) the magnetic field has a strength of a few mG and is usually ordered (Szymczak et al. 2001; Richards et al. 2004). In the case of post-AGB stars, ordered magnetic fields of such a strength may have a dynamical role in shaping the circumstellar outflows, i.e. the magnetic pressure is comparable or even higher than the thermal pressure (e.g. Bains et al. 2003). Soker and collaborators in a series of papers (Soker & Clayton 1999; Soker 2002; Soker & Kastner 2003) argued that the magnetic field is dynamically important in only small parts of the circumstellar envelope; (i) facilitating the formation of dust or (ii) heating and accelerating the gas clumps by the energy released in reconnection events. Similar mechanisms may apply in RSGs though the physical conditions are somewhat different.

Using the long-term observations of two RSGs S Per and VX Sgr reported in this paper, we aim to characterize the OH emission in full polarization and to search for events which can be related to local effects of the magnetic field. Both targets are semiregulars with mean visual periods of 832 and 732 days (Kholopov et al. 1987). Their general properties were summarized elsewhere (Szymczak & Cohen 1997; Richards et al. 1999; Lekht et al. 2005). Optical and near-infrared images of high resolution showed a slight deviation from circularity (Monnier et al. 2004; Schuster et al. 2006).

In the standard circumstellar envelope model (e.g. Habing 1996, for review), the different masers are located in concentric, spherical shells. High angular resolution observations reveal a more complicated picture, which could be due to poor filling, deviations from symmetry or both. The 1665/1667 MHz lines in S Per and VX Sgr arise from regions overlapping the H_2O masers (Chapman & Cohen 1986; Richards et al. 1999, 2007). The inner radius of the OH mainline maser shells is typically around 100 AU from the star, around the middle of the H_2O shell, but

⋆ Appendices A and B are only available in electronic form via http://www.edpsciences.org
⋆⋆ A complete catalogue of the data in all four Stokes parameters is only available in electronic form at CDS via anonymous ftp to cdsarc.u-strasbg.fr (130.79.128.5) or via http://cdsweb.u-strasbg.fr/viz-bin/qcat?J/A+A/524/A99

they extend to several hundred AU, 2–5 times the outer limit of H_2O masers. These OH masers have a patchy and asymmetric distribution and interleave the H_2O clumps in the overlap zone. The 1612 MHz line arises in the outer regions of 600–1400 AU from the central star (Szymczak et al. 1997; Masheder et al. 1999; Richards et al. 2004). Thus, when observing the 1667 and 1612 MHz lines, we probe the OH maser behaviour at different depths of the envelopes.

2. Observations

Full polarization spectra at 1667.359 and 1612.231 MHz were taken with the Nançay radio telescope (NRT) using the observing system, autocorrelator setup and calibration procedure identical to that described in Szymczak & Gérard (2004). The Stokes spectra I, Q and V were directly measured with the system, while the parameter U was extracted by a horn rotation by 45°. The linearly polarized flux density was defined as $p = \sqrt{Q^2 + U^2}$. The degrees of circular polarization, $m_C = V/I$, linear polarization, $m_L = p/I$, and position angle, $\chi = 0.5\times\tan^{-1}(U/Q)$, were derived from the Stokes parameters.

The spectral resolution was 0.14 km s^{-1} and velocity coverage was 70 km s^{-1}. A typical 1σ noise level in the Stokes I spectrum was 40 mJy. The absolute and relative accuracies of the gain in each polarization channel were ∼5% and ∼2% and the absolute flux density scale was accurate to within 7–8%. The error in polarized intensity due to polarization leakage between the orthogonal feeds measured with calibration sources is ∼1%.

S Per and VX Sgr were observed at 36 (2002–2005) and 74 (2002–2008) different epochs, respectively. Both targets were sampled at irregular intervals of 2–3 days up to 4 months. In order to quantify the variability of OH maser emission we calculated a variability index following Goedhart et al. (2004):

$$vi = \Big(\sum_{i=1}^{N}(m(t_i) - \overline{m})^2 - \sum_{i=1}^{N}(n(t_i) - \overline{n})^2\Big)\Big/\overline{m} \quad (1)$$

where N is the total number of observations, $m(t_i)$ is the observed flux density at a given spectral channel at t_i epoch, $n(t_i)$ is the flux density at any emission-free spectral channel at t_i epoch, $\overline{m}$ and $\overline{n}$ are the average flux densities.

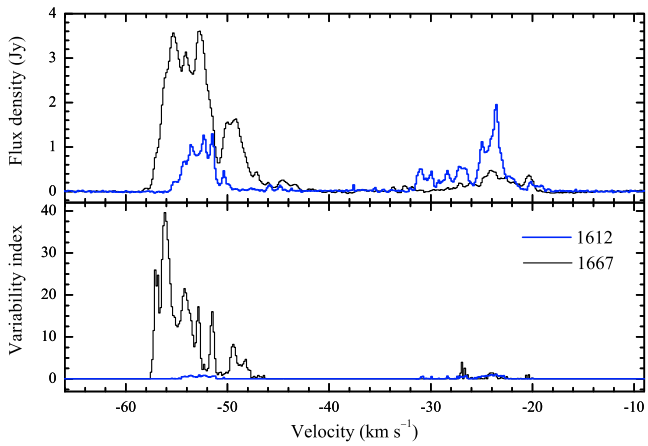

Fig. 1. S Per. The grand average Stokes I spectra at 1612 and 1667 MHz for period March 2002–December 2005 and the corresponding spectra of variability index.

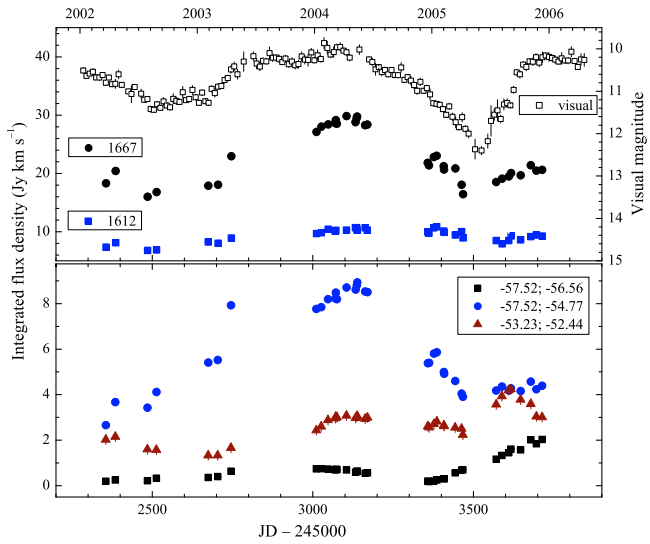

Fig. 2. S Per. *Top panel*: The variations of the integrated OH flux densities (Stokes I) at 1612 and 1667 MHz. The visual mean curve (from AAVSO) with 10 day bins is added. *Bottom panel*: The variations of 1667 MHz flux density integrated over the selected velocity ranges indicated by symbols.

3. Results

Full polarization OH data at 1667 and 1612 MHz of S Per and VX Sgr are shown in Figs. A.1–A.7 and Figs. B.1–B.12, respectively, as plots of the I, V and p flux densities, degrees of polarization m_C, m_L and polarization position angle χ, versus time and velocity. No plots of polarization parameters are shown when the polarized fluxes were below 3σ.

3.1. S Per

3.1.1. S Per 1667 MHz

The 1667 MHz average total intensity spectrum is highly asymmetric; the peak flux ratio of the blue-shifted to the red-shifted profiles is 8.5 (Fig. 1). The extent of the 1667 MHz emission overshoots that of the 1612 MHz emission by 2.8 km s^{-1} in the blue-shifted part of the spectrum and is constant over the period of monitoring. The variability index of the 1667 MHz emission at the extreme velocities, i.e. lower than −55.7 km s^{-1}, is generally higher than 20 (Fig. 1). The variability index steeply decreases in the inner part of the 1667 MHz spectrum down to ∼0.5 for velocities higher than −46 km s^{-1}. The red-shifted profile at 1667 MHz shows weak changes, with *vi* commonly lower than 1.

Variations of the integrated total flux, $S_{\rm int}$, at 1667 MHz roughly follow the visual light curve (Fig. 2). In order to estimate a peak of the light curve in the observed period a polynomial of second order was fitted to the data points ranged from MJD = JD–2450000 = 2950 to 3200 where the putative maximum occurred. The same procedure was applied for the integrated flux densities at 1667 and 1612 MHz. The time of visual maximum is MJD = 3076 ± 6. The 1667 MHz integrated emission is delayed by 26 ± 5 days with the respect of the visual minimum. The relationship with the visual light curve for various 1667 MHz features differ significantly. The bottom panel of Fig. 2 shows variations of the 1667 MHz flux integrated over selected velocity ranges of the blue-shifted parts of the spectrum. The emission at the extreme blue-shifted velocity interval shows changes

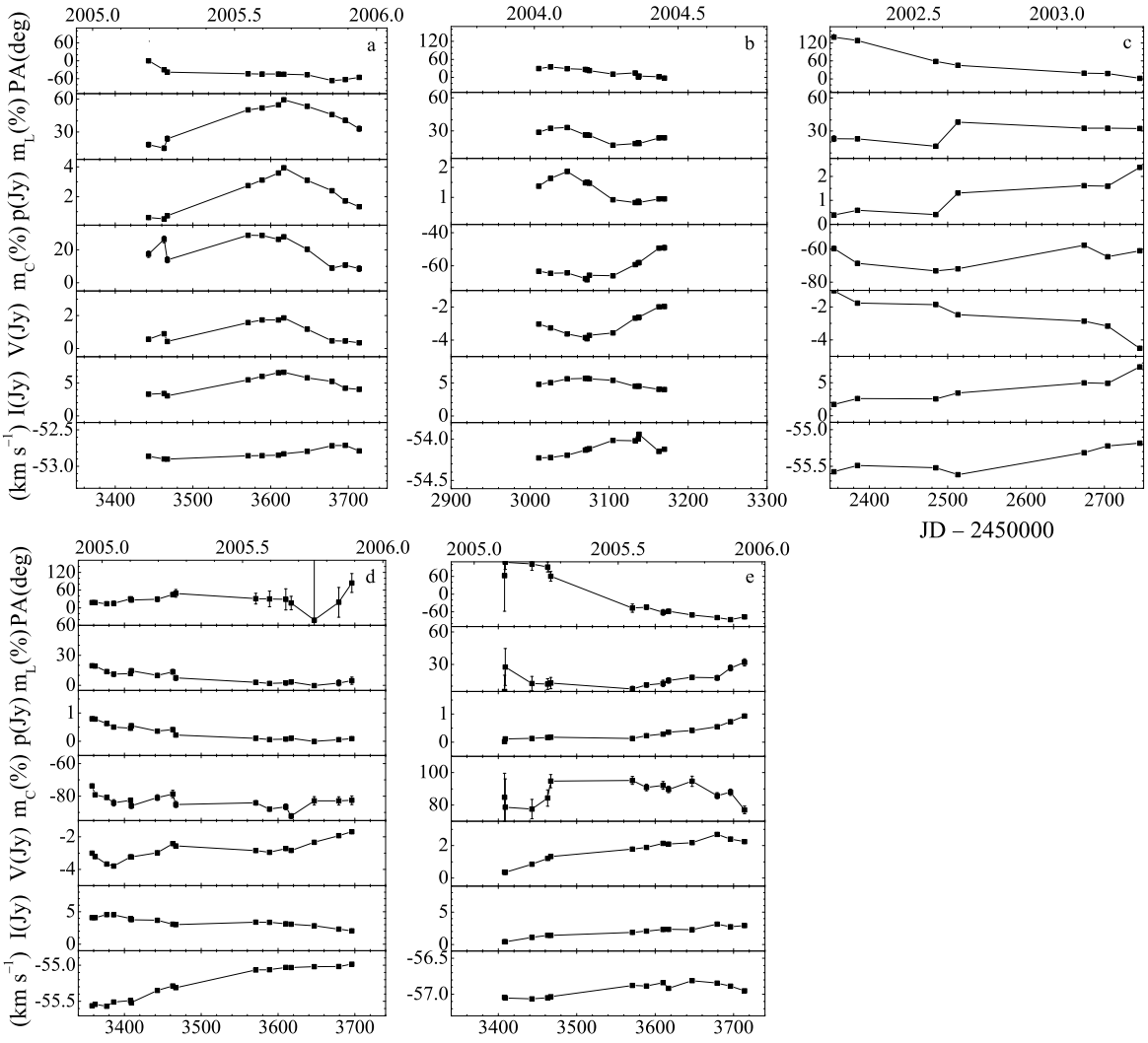

Fig. 3. S Per. Temporal behaviour for five prominent outbursting features at 1667 MHz with central velocities at **a)** −52.9 km s^{-1}; **b)** −54.1 km s^{-1}; **c)** −55.4 km s^{-1}; **d)** −55.3 km s^{-1}; **e)** −56.9 km s^{-1}. For each feature from the bottom to top panels are shown the drifts in velocity, Stokes I flux, Stokes V flux, degree of circular polarization m_C, linearly polarized flux p, degree of linear polarization m_L, and polarization PA.

completely uncorrelated with the visual light curve while for the remaining velocity intervals the time lags range from 38 to 52 days. Erratic behaviour of the total 1667 MHz emission is also observed for the red-shifted velocities (Fig. A.1).

The 1667 MHz features are almost always polarized with $|m_C| \leq 100\%$ and $m_L \leq 85\%$ (Figs. A.2–A.5). The linearly polarized emission is detected only in the blue-shifted part of the 1667 MHz spectrum (Fig. A.3). The degrees of polarization and PA of linear polarization show diverse variability behaviour (Figs. A.5–A.6) on time scales from 0.5 to 4 yr and are usually uncorrelated with the total OH flux and visual light curve. The circularly polarized emission at some velocities shows reversals of polarity (Fig. A.2).

3.1.2. S Per 1612 MHz

The 1612 MHz average total intensity spectrum is roughly symmetric and the whole profile shows only weak variations with $vi < 1$ (Fig. 1). Variations of $S_{\rm int}$, at this frequency crudely follow the visual light curve (Fig. 2). The time lag between the visual maximum (MJD = 3076 ± 6) and the 1612 MHz integrated flux maximum is 43 ± 11 days. The shape of the 1612 MHz profile, in contrast to the 1667 MHz line, is very stable over the period of observations (Fig. A.7). No polarized emission with a peak flux greater than 0.2 Jy was detected.

The amplitude of $S_{\rm int}$ variations defined as $\log(S_{\rm int}(\max)/S_{\rm int}(\min))$ is 0.20. These small amplitude variations and the relatively scarce sampling of the OH emission prevents us from obtaining a reliable value for the red-blue phase lag which would otherwise provide a distance-independent measure of the OH shell diameter.

3.1.3. S Per outbursting features at 1667 MHz

There are several features at 1667 MHz which show velocity drifts and peculiar variations in the total and polarized flux densities (Figs. A.1–A.3). The behaviour of the most outstanding examples is shown in Fig. 3. The mean velocity, $\langle v \rangle$, drift of velocity, $\Delta v/t$, relative flux amplitudes for Stokes I, V, p, i.e. ΔS_I, ΔS_V, ΔS_p, duration of event, δt, time of maximum (whenever seen), $t_{\max}$, maxima and minima of m_C and m_L, and PA at start and end of event are derived (Table 1). Here ΔS_X is defined as $(S_X(\max) - S_X(\min))/S_X(\min)$, where $S_X(\max)$ and $S_X(\min)$ are the peak flux density for Stokes X in maximum and minimum, respectively. $t_{\max}$ is given in MJD for the bursts. The velocity drift is estimated from a slope of the line fitted to the data.

Table 1. Observational characteristics of bursting features of S Per at 1667 MHz.

feature	$\langle v \rangle$ (km s^{-1})	$\Delta v/t$ (km s^{-1} yr^{-1})	ΔS_I	δt (day)	t_{max} (MJD)	ΔS_V	m_C(max; min) (%)	ΔS_p	m_L(max; min) (%)	PA(start; end) (deg)	type
a	−52.9	0.20	1.00	310	3620	2.88	+29; +9	5.12	57; 18	–27; –60	burst
b	−54.1	0.40	0.43	194	3070	0.91	–68; –49	1.23	33; 17	37; –1	burst
c	−55.4	0.35	3.29	391	–	3.46	–73; –58	5.10	33; 23	138; 2	rise
d	−55.3	0.67	1.19	340	–	1.29	–89; –79	7.78	18; 1	18; 40	decline
e	−56.9	0.22	6.05	306	–	6.06	+95; +86	7.90	30; 18	104; –85	rise

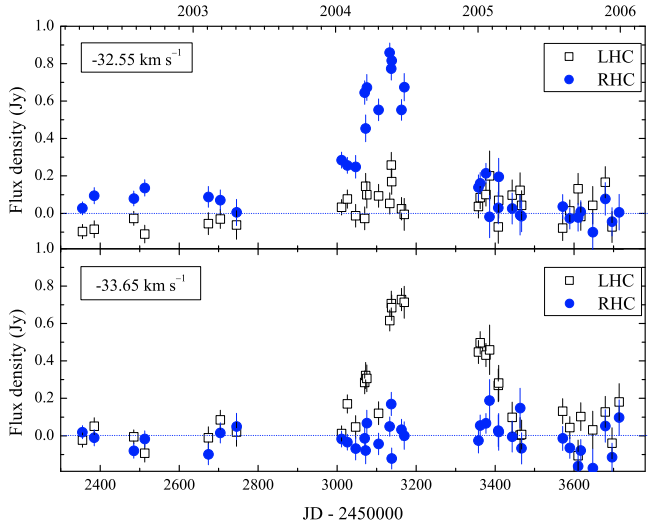

Fig. 4. S Per. Two outbursts of completely circularly polarized emission at 1667 MHz.

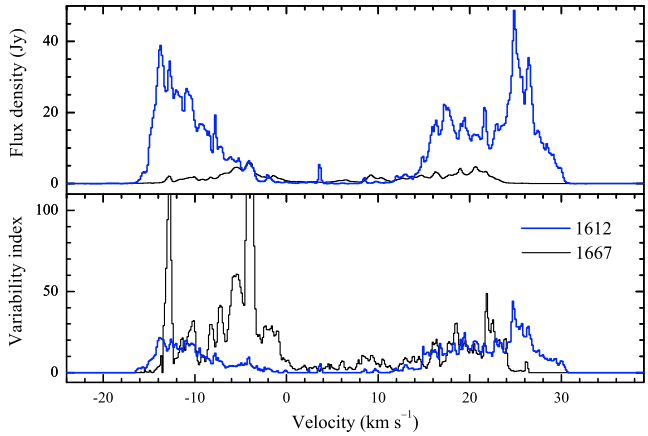

Fig. 5. VX Sgr. The grand average Stokes I spectra at 1612 and 1667 MHz for period October 2002–December 2008 and the corresponding spectra of variability index. Variability index peaks not shown for 1667 MHz features near −12.8 and −3.9 km s^{-1} are 154 and 227, respectively.

The type of event (Table 1) is defined solely by the variations of Stokes I flux density. The features near −52.9 and −54.1 km s^{-1} show clear outbursts on time scales of 6–10 months. The velocity drifts of $\lesssim$0.22 km s^{-1} are possibly blending effects due to variability of one feature in a crowded part of the spectrum. Three other features near −55.3, −55.4 and −56.9 km s^{-1} appear to be observed after or before a burst that possibly is longer than one year. The time scales of the 1667 MHz outbursts are shorter than the optical period of 822 days (Kholopov et al. 1987), but may be comparable with the secondary cycle of 300–700 days. All the features analyzed have usually $|m_c| > 50\%$ and $m_L < 30\%$ which show only moderate (<20%) variations. A clear trend of decrease in P.A. of linear polarization is seen in four features.

A faint unpolarized feature of 0.18 Jy (~4σ) at 1667 MHz was detected near −61.2 km s^{-1} at all three occasions in 2003 (Fig. A.1). The weak ($\leq$70 mJy beam^{-1}) emission at more extreme velocities from −63 to −65 km s^{-1} reported in Richards et al. (1999, 2004) was never detected with the NRT, possibly due to lower (6–8 times) sensitivity. In the red-shifted part of the 1667 MHz spectrum a burst of fully circularly polarized emission occurred in 2004 (Fig. 4, see also Fig. A.2). A Gaussian fit analysis yields that the burst in the right-hand circular (RHC) polarized emission near −32.55 km s^{-1} had amplitude of 0.74 Jy at MJD = 3159 ± 8 and lasted 381 days. The burst of the left-hand circular (LHC) polarized emission near −33.65 km s^{-1} of 1.05 Jy amplitude reached a maximum at MJD = 3241 ± 3 and lasted 402 days. These estimates for the LHC emission seem more reliable than for the RHC emission because the rise and decline are clearly visible for the former.

Figure A.1 clearly shows the appearance of a dip in the 1667MHz spectrum near −56.1 km s^{-1} since MJD = 3358. Its velocity drift derived over the period of 306 days is 1.26 km s^{-1} yr^{-1}.

We note that the 1667 MHz outbursts near −52.9 and −32.55/−33.65 km s^{-1} occurred at the optical maximum, whereas the other events were observed during the optical minima. In all the long lasting ($\gtrsim$1 yr) bursts the 1667 MHz emission was highly polarized. While the 1667 MHz emission, especially in the blue-shifted part of the spectrum (<−48 km s^{-1}) was violently variable, the 1612 MHz emission showed no eruptive activity (Fig. A.7).

3.2. VX Sgr

3.2.1. VX Sgr 1667 MHz

The average 1667 MHz spectrum is complex and roughly symmetric (Fig. 5). It is less extended than the 1612 MHz emission by 1.6 and 6.6 km s^{-1} at the blue- and red-shifted extremes, respectively. The variability index of the blue-shifted emission, in contrast to the red-shifted one, is commonly higher than 20 reaching value as high as 150 for two features (Fig. 5). Variations of S_{int} crudely follow the visual variations (Fig. 6). For the interval of MJD from 3165 to 3814 where a visual minimum occurred and the OH data were best sampled we fitted a second order polynomial to the data points. The time lag between the visual and radio curves at minimum (MJD = 3516.4 ± 4.0) is 68.9 ± 4.2 days. The time lag for the 1667 MHz line is considerably affected by highly variable features as is shown in the bottom panel of Fig. 6. As is the case for S Per, the OH 1667 MHz maser variability of VX Sgr is much higher at blue-shifted velocities than at red-shifted velocities, with a variability

Table 2. Same as in Table 1 but for VX Sgr.

feature	$\langle v \rangle$ (km s^{-1})	$\Delta v/t$ (km s^{-1} yr^{-1})	ΔS_I	δt (day)	t_{max} (MJD)	ΔS_V	m_C(max; min) (%)	ΔS_p	m_L(max; min) (%)	PA(start; end) (deg)	type
a	−3.8	−0.02	6.07	663	3159	4.07	+49; –21	12.7	62; 11	39; 43	burst
b	−4.3	0.22	1.17	620	4070	4.44	–59; 23	1.14	84; 6	5; 57	burst
c	−5.4	0.07	3.52	675	3258	3.20	28; –22	8.67	23; 5	4; 26	burst
d	−11.4	−0.23	1.10	696	3883	1.63	–19; 11	2.14	36; 4	42; 84	burst
e	−12.8	−0.03	3.97	786	4033	6.07	+69; +14	4.29	92; 11	–4; –40	burst

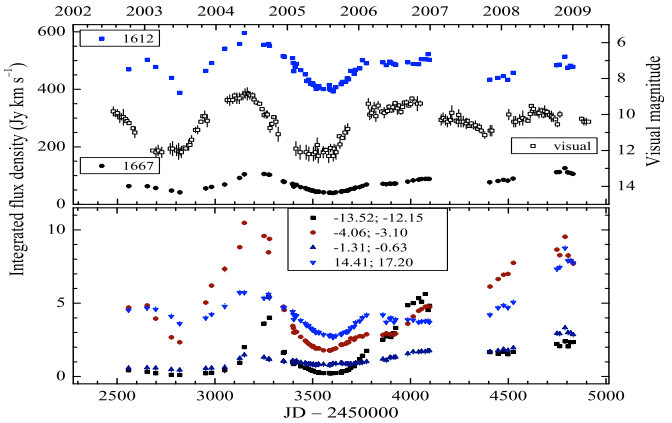

Fig. 6. Same as in Fig. 2 but for VX Sgr.

index above 100 for some features. The average variability index for the blue- and red-shifted sides for VX Sgr is 35.1 and 12.1, respectively, while for S Per is 10.5 and 0.7, respectively.

The blue- and red-shifted 1667 MHz features have $|m_C| < 90\%$ and $m_L < 90\%$, and $|m_C| < 45\%$ and $m_L < 50\%$, respectively. Diverse polarization behaviour (Figs. B.1–B.6) is not correlated with the total flux and visual variations. There are plenty of features which exhibit a reversal of circular polarization on time scales of a few years.

3.2.2. VX Sgr 1612 MHz

The 1612 MHz emission is bright forming a complex and crudely symmetric spectrum (Fig. 5). The variability index is usually lower than 20, with the exception of the velocity range of 24.6–26.7 km s^{-1} where its mean value is 29. Variations of S_{int} fairly follow the visual light curve. We estimated the time of minimum in the MJD range from 3165 to 3814 in the same way as for the 1667 MHz emission. The 1612 MHz integrated emission is delayed by 57.8 ± 4.1 days with respect to the visual minimum (MJD = 3516.4 ± 4.0). Variations of the 1612 MHz emission are clearly less than those at 1667 MHz.

The polarization at 1612 MHz is less pronounced; m_C ranges from −45 to 45% while m_L is usually lower than 25%. For almost all 1612 MHz features the degrees of polarization are stable within about 5% or show monotonic variations over the period of observation (Figs. B.7–B.12).

3.2.3. VX Sgr outbursting features at 1667 MHz

The peculiar bursting nature of the 1667 MHz emission is easily seen in Figs. B.1–B.6. A sample of prominent bursting features for the blue-shifted emission is shown in Fig. 7 and their parameters are listed in Table 2. All the features exhibit only marginal velocity drifts. The duration of the bursts ranges from 620 to 786 days that is comparable with the mean visual period of 732 days (Kholopov et al. 1987) but some features appear to be the superposition of bursts of different durations. For instance the feature near −11.4 km s^{-1} can be composed of at least three bursts lasting 80–150 days, while the bursts near −4.3 and −12.8 km s^{-1} are superimposed on an increase of OH flux lasting up to 2300 days. Maxima of the prominent bursts usually coincide with visual maxima. The degrees of circular and linear polarization show significant variations with amplitude up to 80%. The position angle of linear polarization exhibits smooth changes by 5–52°.

3.2.4. VX Sgr secular variations at 1612 MHz

In general the 1612 MHz emission shows quite smooth variations (Figs. B.7–B.12) without outstanding bursts. To investigate small variations in the OH 1612 MHz flux we performed a least-squares linear fit to the normalized data points (74 epochs) for each channel where the the peak flux was greater than 1 Jy. The same fitting procedure is applied for the visual curve. Over the interval of 2273 days of our observations we find that, despite semi-periodic variations, there is an increase of visual brightness with slope of 0.27×10^{-4}. The difference between the slopes of the best fits for OH flux and visual brightness for each spectral channel is shown in Fig. 8. For the emission in the velocity range from −16 to −2 km s^{-1} we note random changes of slope; thus the OH flux increases or decreases in time from channel to channel but on average the secular variations follow those in the visual. In contrast, the central and red-shifted emission shows a decreasing trend with the exception of the extreme red-shifted emission at 28–30 km s^{-1}, where a steep increase of the OH flux occurs. The steepest decrease is observed for four channels centered at 3.7 km s^{-1} and is seen for others up to 23 km s^{-1}. We conclude, the 1612 MHz profile undergoes measurable changes over a period of 6 yr. A comparison of our data with the published spectra of similar spectral resolution (Chapman & Cohen 1986; Szymczak & Cohen 1997) suggests that a decline in flux in the velocity range 3–23 km s^{-1} and a rise for velocities greater than 23 km s^{-1} persist over 27 yr. These variations are likely to be due to secular changes in the physical conditions related to the passage of the stellar wind across the 1612 MHz maser envelope. The crossing time estimated from the envelope parameters (Szymczak & Cohen 1997) is about 300 yr.

4. Discussion

4.1. Systemic and terminal velocities

The systemic velocity of S Per and the expansion velocity of different layers in the envelope have been estimated in several studies (e.g. Diamond et al. 1987; Richards et al. 1999, 2004). Our

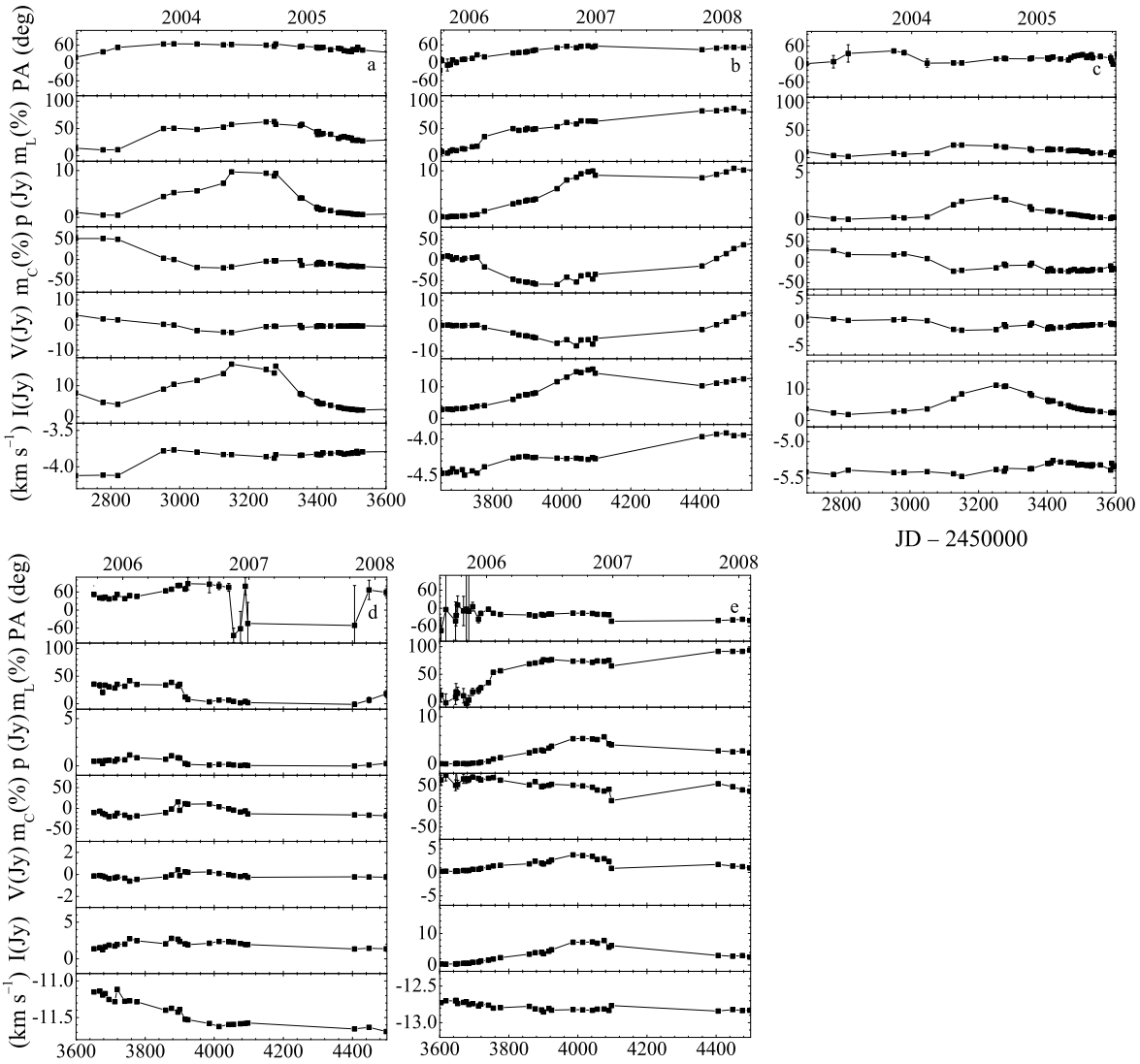

Fig. 7. Same as in Fig. 3 but for VX Sgr and features with central velocities at **a)** −3.8 km s^{-1}; **b)** −4.3 km s^{-1}; **c)** −5.4 km s^{-1}; **d)** −11.4 km s^{-1}; **e)** −12.8 km s^{-1}.

data show that the 1612 MHz profile shape is very stable over a period of 4 yr. The mean velocity of the outer peak features is $V_s = -36.9 \pm 0.2$ km s^{-1} and agrees within ±0.2 km s^{-1} with the constant mid-point of the maximum velocity range of the emission measured at 1σ level. This estimate of the systemic velocity is very close to the value of −37.0 km s^{-1} inferred from the CO(2−1) line (Josselin et al. 1998) but slightly differs from the value of −38.5 ± 0.5 km s^{-1} (Diamond et al. 1987 and references therein) adopted from old 1612 MHz data with a signal to noise ratio lower than ours.

The expansion velocity of the 1612 MHz envelope in S Per defined as the half-maximum width of the OH peak emission is 18.4 ± 0.2 km s^{-1}. It appears to be close to the upper bound of the previously reported range of 14–19 km s^{-1} (Diamond et al. 1987; Richards et al. 1999 and references therein). Observations of the CO(2–1) and (3–2) transitions have yielded an expansion velocity of 17 km s^{-1} (Josselin et al. 1998) and 20 km s^{-1} (Woodhams 1993), respectively. Gonzalez-Alfonso et al. (1998) reported a terminal velocity of 24.6 km s^{-1} (their Table 2) from the width of the CO(2–1) profile but their Fig. 2 shows a much lower value of ∼19 km s^{-1}. We conclude that the expansion velocity derived from the 1612 MHz profile is very close to the terminal velocity of outflow in S Per.

The expansion and systemic velocities of VX Sgr inferred from the extent of the 1612 maser emission observed with MERLIN (Szymczak & Cohen 1997) are 21.4, and 6.2 ± 0.4 km s^{-1}, respectively, whereas the present NRT data rather imply 23.9 and 6.9 ± 0.2 km s^{-1}. When comparing their profile with ours, taken ≳10 yr later, we note a 1.0 km s^{-1} broadening at the extreme red-shifted velocity. Figs. B.7–B.8 show the appearance of weak (0.3–0.5 Jy) emission at velocities higher than 30.2 km s^{-1} since 2003.85 (MJD = 2953) that persisted over the rest of the observations. This suggests that the new 1612 MHz emission arises in the outermost regions of the envelope which are still weakly accelerating.

4.2. Departure from symmetric outflow in S Per

The present study clearly shows that the 1667 MHz emission consists of bursting components at velocities lower than −55.6 km s^{-1}, i.e. beyond the velocity range of the 1612 MHz emission. In addition the bursting 1667 MHz feature near −61.2 km s^{-1} detected here and features from −63 to −65 km s^{-1} reported in Richards et al. (1999) have velocities 5.8–9.6 km s^{-1} higher than the terminal velocity inferred from the 1612 MHz

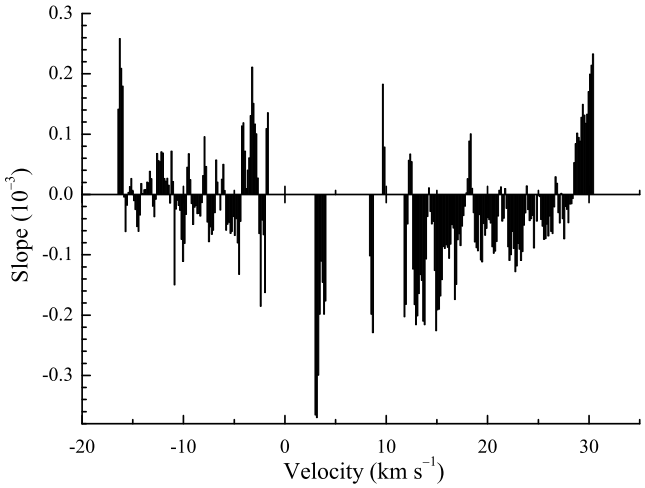

Fig. 8. VX Sgr. Slope of linear fit to the Stokes *I* flux variation over the entire observing period at 1612 MHz corrected for the slope of the linear fit to the visual brightness variation. Channels with peak flux greater than 1 Jy are shown.

profile. A H_2O 22 GHz maser feature near −57 km s^{-1} (Marvel 1996; Gonzalez-Alfonso et al. 1998) also slightly (1.4 km s^{-1}) exceeds the terminal velocity. VLBI and MERLIN maps show that the OH emission in all lines is elongated NE−SW (Masheder et al. 1999; Richards et al. 1999, 2004). A similar elongation is also seen in the high resolution images at 0.47 μm (Schuster et al. 2006) and 2.0–2.4 μm (Thompson & Creech-Eakman 2003). The brightest H_2O maser hotspots detected by the VLBA have a similar distribution (Marvel 1996; Vlemmings et al. 2001) with the greatest proper motions along PA ∼40°. However, more sensitive 22 GHz observations show that the H_2O maser shell is almost spherical (Richards et al. 1999).

The asymmetric appearance of the envelope and the presence of fast maser components cannot be easily explained with the model of bipolar outflow originally proposed for AGB stars (e.g. Zijlstra et al. 2001, and references therein). In this model a bipolar morphology is predicted from the interaction of slow and fast stellar winds. The main argument against this model is that the star has an effective temperature of about 3500 K (Levesque et al. 2005; Verhoelst et al. 2009), thus it is too cool to produce fast winds. The OH and H_2O masers of many Miras usually show an apparent asymmetry with a preferred axis. The infrared colours of Miras are very similar to those of RSGs. Especially, S Per has relatively warm, young IRAS colours and faint 1612 MHz emission which might suggest a relatively young shell which has not yet become fully filled. Its H_2O maser envelope has a slight asymmetry along the axis of strongly polarized OH maser spots (Richards et al. 2004). It seems likely that the observed asymmetry is a combined effect of poorly filled shell and the stellar magnetic field. The same appears to be true for VX Sgr where H_2O maser envelope is spheroidal with a slight asymmetry (Murakawa et al. 2003) along the magnetic field direction inferred from the OH 1612 MHz masers (Szymczak et al. 1997) and H_2O masers (Vlemmings et al. 2001).

4.3. Locations of active regions in S Per

An inspection of MERLIN and VLBI maps (Masheder et al. 1999; Richards et al. 1999, 2004) implies that the brightest main line OH emission arises from within ≲20 mas of the line of sight towards the assumed stellar position. Specifically, in the most recent data taken with MERLIN in 1999 the brightest, most variable and most strongly polarized components at 1667 MHz come from the front-side of the envelope at blue-shifted velocities below −48 km s^{-1}, with a mean flux-weighted angular distance from the assumed stellar position, of 6.2 mas (Richards et al. 2004). Our NRT data obtained more than 3 years later also show that the strongest 1667 MHz emission appears in the same velocity range where all but one outburst emerged. The time taken for material to travel out through the 1667 MHz OH envelope of 140 AU radius is about 40 yr (Richards et al. 1999). MERLIN observations of the OH mainlines in 1993 and 1999 show a similar NE−SW elongation, as do the two epochs of OH 1612-MHz imaging. The overall structure of the OH envelope as seen with MERLIN was likely preserved during our monitoring period. It is also important that the blue-shifted main line emission is almost always brighter than the red-shifted (Baudry et al. 1977; Richards 1997). We argue that the active region with the strongest 1667 MHz emission and bursting features has a mean radius of about 3 times (with a maximum of almost 10 times) larger than the stellar radius of S Per (Thompson & Creech-Eakman 2003). Considering a size of the radio-photosphere a factor of two higher than the optical photosphere at least in AGB stars (Reid & Menten 1997a), we surmise that a contribution of the stellar background photons to amplification of the 1667 MHz maser emission is highly likely for the active region. Although the optical variation time scale of 2−3 years is comparable with the time scale of some of the OH outbursts, the flux variations of the burst features do not follow the visual light curve.

4.4. Long-term variations of S Per and VX Sgr

Our observations revealed fairly smooth low amplitude variations of the 1612 MHz flux density from S Per which are moderately correlated with the optical light curve. We note that the OH profile has changed very little since 1993 (Richards 1997) and had a similar shape and intensity as in 1974 (Baudry et al. 1977). Inspection of the literature suggests that the apparently fainter red-shifted emission at some epochs is due to lower spectral resolution since the peak is narrower at high spectral resolution and is fainter when averaged over lower resolution. Furthermore, the non-detection of some of the fainter features at earlier epochs seems to be a result of lower sensitivity. We argue that the 1612 MHz profile of S Per does not show substantial changes on time scale of ∼30 yr while its intensity follows semiregular optical variations.

Our six year monitoring of VX Sgr has shown that the integrated 1612 MHz emission has small amplitude variations that follow the optical light curve, whilst the spectral profile is generally well preserved. Periodic changes of the 1612 MHz and infrared fluxes were reported from observations taken in the period of 1969–1972 (Harvey et al. 1974). Comparison with data obtained in 1993–1995 (Richards 1997) suggests that the 1612 MHz profile is very similar in shape and intensity with the exception of extreme blue- and red-shifted peaks. Further inspection of old data (e.g. Masheder et al. 1974; Chapman & Cohen 1986; Szymczak et al. 1997, 2001) implies that the profile shape is generally stable on time scale of ∼40 yr, with the exception of some extreme blue- and red-shifted parts.

Semiregular and smooth variations of the 1612 MHz emission in both RSGs following the optical light curves are similar to the OH and optical/infrared light curves obtained for many late-type objects (e.g. Harvey et al. 1974; Herman 1985;

Herman & Habing 1985; Chapman 1988; West et al. 1992; Gaylard & West 1995; Etoka & Le Squeren 2000; Whitelock et al. 2008). The correlated variations of OH and far-infrared fluxes are consistent with the model of the radiative pumping of the 1612 MHz OH line by far-infrared photons that was ultimately confirmed by *ISO* observations (e.g. Sylvester et al. 1997). The time delay of 43–58 days of the 1612 MHz flux with regard to the visual variation is observed in the two RSGs. Relatively high errors of the OH maximum determination and poorly defined visual maxima in both RSGs certainly affect the estimates of the time lags. Further uncertainty in the phase lag determination of the maser light curves with respect to the visual light curves is due to the light travel time from the star to the blue and red wings of the OH profiles. This is particularly true at 1612 MHz where the envelopes have a larger size than at 1667 MHz. Despite of a large uncertainty of the phase lag we note that a light travel distance of 50 days corresponds to a linear distance of $\sim 1.3 \times 10^{17}$ cm which is reasonably consistent with the expected diameter for the OH 1612 MHz envelope of a RSG.

The 1667 MHz integrated flux of S Per roughly follows the optical variations but the individual features show large variability making the whole profile shape very different on time scale 0.5–1.0 yr. High variability of the main line OH masers was also reported in Richards (1997); her spectra taken in 1993–1994 are generally different from ours, but a tendency that the blue-shifted emission is dominant is preserved. The 1667 MHz spectrum taken in 1982 (Diamond et al. 1987) illustrates dramatic difference in the shape; the strongest features occurred near -40 km s^{-1} just in the middle of the profile reported here and Richards (1997). We find that the intensity and shape of 1667 MHz profile of S Per shows significant long term (3–25 yr) changes.

The behaviour of the 1667 MHz emission of VX Sgr resembles that observed in S Per; the integrated flux density generally follows the visual variations but individual features have much less regular variations which are less directly related to the stellar cycle. The spectra from 1993–1995 reported by Richards (1997) are severely different from ours and do not resemble those obtained in 1983 (Chapman & Cohen 1986). We find that the 1667 MHz line profile of VX Sgr has extremely large variability on time scales of 2–25 yr.

Althought there are systematic relationships between the stellar and OH maser brightness such as illustrated in Figs. 2 and 6 we argue that they cannot explain all the variability observed, especially at 1667 MHz. In particular at this frequency the degrees of circular and linear polarization show irregular variations commonly uncorrelated with the total OH flux. Furthermore, the emission in several channels shows a reversal of the sign of circular polarization. We note that the inner envelope where the 1667 MHz originates is probably more turbulent than the outer 1612 MHz envelope. In consequence, local changes of path length, pump rate, magnetic field could affect the maser intensity. In the 1612 MHz outer envelope are probably more homogeneous conditions and variations of the OH flux are more regular.

4.5. Origin of the outbursts

Interferometric maps of S Per show that the H_2O 22 GHz masers are concentrated in clumps and maser theory suggests that they have a typical density of $\sim 3 \times 10^{11}$cm^{-3}, while the OH 1665/1667 MHz masers likely come from lower density intercloud gas. Although the components of both maser species avoid each other in position and velocity it appears the OH main line masers emerge at a similar distance from the star, but extend further (Masheder et al. 1999; Richards et al. 1999, 2004). Similarly, in VX Sgr, the OH 1665/1667 MHz maser shell has an inner radius overlapping the H_2O masers (Chapman & Cohen 1986) but extends to near the 1612 MHz masers (Richards et al. 2008). In such a case some mechanisms of variability may be common to both species.

Shock waves driven by stellar pulsations are postulated as possible causes of H_2O variations in S Per (Lekht et al. 2005). In this model an increase of integrated H_2O flux detected at a given epoch should be correlated with one of the previous visual maxima depending on the shock travel time from the stellar surface to the maser layers. For instance, a shock of velocity $\sim$10 km s^{-1} affects the H_2O and OH maser region $\sim$40 yr later (Richards et al. 1999; Lekht et al. 2005). An inspection of the AVVSO data from interval of 60–30 yr earlier than our observations failed to show any correlation.

The observations of S Per show that much of the OH mainline emission was resolved out by the EVN and a lower limit to the average OH cloud radius is $\sim$9 AU with a maximum of almost 30 AU (Richards et al. 2004). The disturbances of velocity 10 km s^{-1} propagate across such an average clump over about 8.5 yr. This time scale is about 10 times longer than the typical duration of the 1667 MHz outbursts observed in S Per. This does not necessarily exclude shocks as the cause of burst activity of the 1667 MHz maser. Although theoretical models predict shock induced changes of the velocity field of outflowing gas at time scales of a few months (e.g. Hofner et al. 1995) the study of shock waves in long period variable stars by Reid & Menten (1997b) have shown that period shocks at distance of a few stellar radii propagate outward with slow velocity ($\sim$5 km s^{-1}) and/or are mostly damped. Therefore, it is unlikely that shock waves have much influence at distances of the H_2O and OH masers in a circumstellar envelope. We note that even quite small velocity disruptions, of order the thermal line width of 1.5 km s^{-1}, could suppress or enhance unsaturated maser dramatically.

Our data for S Per show apparent velocity drifts of the 1667 MHz features; all features (Table 1) exhibit the same drift direction. The variability of features with a velocity drift $\leq$0.3 km s^{-1} yr^{-1} is possibly due to blending of two or more spectral features. This is clearly seen for feature -52.9 km s^{-1} (Table 1) where the difference in velocity after and before burst is $\sim$0.1 km s^{-1}. On the other hand, there are examples of features such as -55.4 km s^{-1} for S Per (Table 1, Fig. 3) and -11.4 km s^{-1} for VX Sgr (Table 2, Fig. 7) which likely represent real velocity shifts of maser clouds. Velocity drifts of the individual features of H_2O maser emission were reported for a sample of 46 AGB stars (Shintani et al. 2008). They are consistent with accelerated/decelerated motions. Velocity drifts have previously been recorded in a long-term monitoring study of H_2O masers associated with star formation regions and bright-rimmed clouds (e.g. Brand et al. 2003) which are interpreted as being due to acceleration/deceleration of the maser clouds. We suggest that the velocity drifts detected in the blue-shifted emission of S Per are more likely due to the deceleration of real physical blobs than to the passage of shock waves. In the blue-shifted emission of VX Sgr we observed the velocity drift of feature *d* which appears to be consistent with an outward acceleration.

There is observational evidence that the OH maser (also H_2O and SiO) components trace real physical blobs or clumps. If the two RSGs studied here are undergoing multiple and asymmetric mass-loss events one can suspect that the OH outburst

phenomena may be related to individual clumps. Discrete mass loss in the form of complex ejects of arcs and knots were clearly detected in the supergiant star VY CMa (Humphreys et al. 2007). Asymmetric ejections and multiple high mass loss events were observed in post-RSG IRC+10420 while large scale asymmetry was seen in the optical nebulosity around NML Cyg supergiant (Schuster et al. 2006). The complex ejecta of arcs and knots observed and multiple mass loss events probably involve large-scale convection and magnetic fields. It has been shown that the arcs are too massive to have been driven by radiation pressure alone. The localized mass ejections may be due to enhanced dust formation above cool magnetic spots (Soker & Clayton 1999) and/or magnetic reconnection events near the stellar surface (Soker & Kastner 2003) as originally proposed for AGB stars. Similar mechanisms likely work for RSGs. As the reconnection process is basically cancellation of the field lines of opposite directions whereas the energy released heats and accelerates the gas, the clumps reaching the maser regions would have well organized magnetic fields and velocities higher than expected by radiation pressure alone. This seems to be consistent with small variations of the degrees of polarization and smooth changes of PA of linear polarization during the bursts of individual highly polarized features detected in the targets. We suggest that the small-scale magnetic field topology of the flaring region can play a role in the spatial and temporal development of the localized OH maser emission.

5. Conclusions

The 1612 and 1667 MHz OH masers from two supergiants S Per and VX Sgr were monitored in all Stokes parameters over 4 and 6 yr, respectively. Variations of the integrated flux density of both OH lines are correlated with the visual light curves but some individual features largely varied independently, especially those at 1667 MHz. A number of features showed the velocity drifts of more than 0.3 km s^{-1} yr^{-1} indicating acceleration and deceleration of maser clouds. Bursts of highly polarized emission on time scales of 0.5–2 yr occurred in the 1667 MHz line. Their polarization characteristics for S Per were relatively stable suggesting the presence of magnetic field that may be locally involved in OH outbursts at distances of 140–200 AU from the central stars but for VX Sgr they were largely variable. The 1612 MHz emission does not show bursting activity but in VX Sgr it exhibits secular changes.

A complete catalogue of the data in all four Stokes parameters can be found at the CDS.

Acknowledgements. The Nancay Radio Observatory is the Unité Scientifique de Nancay of the Observatoire de Paris, associated with the CNRS. The Nancay Observatory acknowledges the financial support of the Region Centre in France. We acknowledge with thanks the AAVSO International Database, which is based on observations submitted to the AAVSO by variable-star observers world-wide.

References

Bains, I., Gledhill, T. M., Yates, J. A., & Richards, A. M. S. 2003, MNRAS, 338, 287
Baudry, A., Le Squeren, A. M., & Lepine, J. R. D. 1977, A&A, 54, 593
Brand, J., Cesaroni, R., Comoretto, G., et al. 2003, A&A, 407, 573
Chapman, J. M. 1988, MNRAS, 230, 415
Chapman, J. M., & Cohen, R. J. 1986, MNRAS, 220, 513
Cohen, R. J., Downs, G., Emerson, R., et al. 1987, MNRAS, 225, 491
Diamond, P. J., Johnston, K. J., Chapman, J. M., et al. 1987, A&A, 174, 95
Etoka, S., & Le Squeren, A. M. 2000, A&AS, 146, 179
Gaylard, M. J., & West, M. E. 1995, ASPC, 83, 411
Goedhart, S., Gaylard, M. J., & van der Walt, D. J. 2004, MNRAS, 355, 553
Gonzalez-Alfonso, E., Cernicharo, J., Alcolea, J., & Orlandi, M. A. 1998, A&A, 334, 1016
Habing H. J. 1996, A&AR, 7, 97
Harvey, P. M., Bechis, K. P., Wilson, W. J., & Ball, J. S., 1974, ApJS, 27, 331
Herman, J. 1983, Ph.D. Thesis, University of Leiden
Herman, J., & Habing, H. J. 1985, A&AS, 59, 523
Hofner, S., Feuchtinger, M. U., & Dorfi, E. A., 1995, A&A, 297, 815
Humphreys, R. M., Helton, L. A., & Jones, T. J. 2007, AJ, 133, 2716
Josselin, E., Loup, C., Omont, A., et al. 1998, A&AS, 129, 45
Kholopov, P. N., et al. 1987, General Catalogue of Variable Stars, 4th ed. (Moscow: Nauka), III, 30
Lekht, E. E., Rudnitskij, G. M., Mendoza-Torres, J. E., & Tolmachev, A. M. 2005, A&A, 437, 127
Levesque, E. M., Massey, P., Olsen, K. A. G., et al. 2005, ApJ, 628, 973
Marvel, K. B. 1996, Ph.D. Thesis, New Mexico State University
Masheder, M. R. W., Booth, R. S. & Davies, R. D., 1974, MNRAS, 166, 561
Masheder, M. R. W., van Langevelde, H. J., Richards, A. M. S., Greenhill, L., & Gray, M. D. 1999, New A Rev., 43, 563
Monnier, J. D., Millan-Gabet, R., Tuthill, P. G., et al. 2004 ApJ, 605, 436
Murakawa, K., Yates, J. A., Richards, A. M. S., & Cohen, R. J. 2003, MNRAS, 344, 1
Reid, M. J., & Menten, K. M. 1997a, ApJ, 476, 327
Reid, M. J., & Menten, K. M. 1997b, Ap&SS, 251, 41
Richards, A. M. S., 1997, Ph.D. Thesis, University of Manchester
Richards, A. M. S., Yates, J. A., & Cohen, R. J. 1999, MNRAS, 306, 954
Richards, A. M. S., Masheder, M. R. W., van Langevelde, H. J., et al. 2004, in Proc. 7th European VLBI Network Symposium, ed. R. Bachiller, F. Colomer, J. F. Desmurs, & P. de Vicente (Toledo), 209
Richards, A. M. S., Bains, I., Bartkiewicz, A., et al. 2007, in Astrophysical Masers and their Environments, IAUS, 242, 261
Richards, A., Bains, I., Bartkiewicz, A., et al. 2008, in Proc. 9th European VLBI Network Symposium (Bologna), 35
Schuster, M. T., Humphreys, R. M., & Marengo, M. 2006, ApJ, 131, 603
Shintani, M., Imai, H., Ando K., et al. 2008, PASJ, 60, 1077
Soker, N. 2002, MNRAS, 336, 826
Soker, N., & Clayton, G. C. 1999, MNRAS, 307, 993
Soker, N., & Kastner, J. H. 2003, ApJ, 592, 498
Sylvester, R. J., Barlow, M. J., Nguyen-Q-Rieu, et al. 1997, MNRAS, 291, L42
Szymczak, M., & Cohen, R. J. 1997, MNRAS, 288, 945
Szymczak, M., & Gérard, E. 2004, A&A, 423, 209
Szymczak, M., Cohen, R. J., & Richards, A. M. S. 2001, A&A, 371, 1012
Thompson, R. R., & Creech-Eakman, M. J. 2003, AAS, 203.4907
Verhoelst, T., Van der Zypen, N., Hony, S., et al. 2009, A&A, 498, 127
Vlemmings, W., Diamond, P. J., & van Langevelde, H. J. 2001, A&A, 375, L1
West, M. E., Gaylard, M. J., Combrinck, W. L., Cohen, R. J., & Shepherd, M. C. 1992, ASPC, 30, 277
Whitelock, P. A., Feast, M. W., & van Leeuwen, F. 2008, MNRAS, 386, 313
Woodhams, M. 1993, in ASPC Massive Stars: Their Lives in the Interstellar Medium. ed. J. P., Cassinelli, & E. B., Churchwell, 35, 231
Zijlstra, A. A., Chapman, J. M., te Lintel Hekkert, P., et al. 2001, MNRAS, 322, 280

Pages 10 to 28 are available in the electronic edition of the journal at http://www.aanda.org

Appendix A: Polarization spectra of S Per at 1667 and 1612 MHz

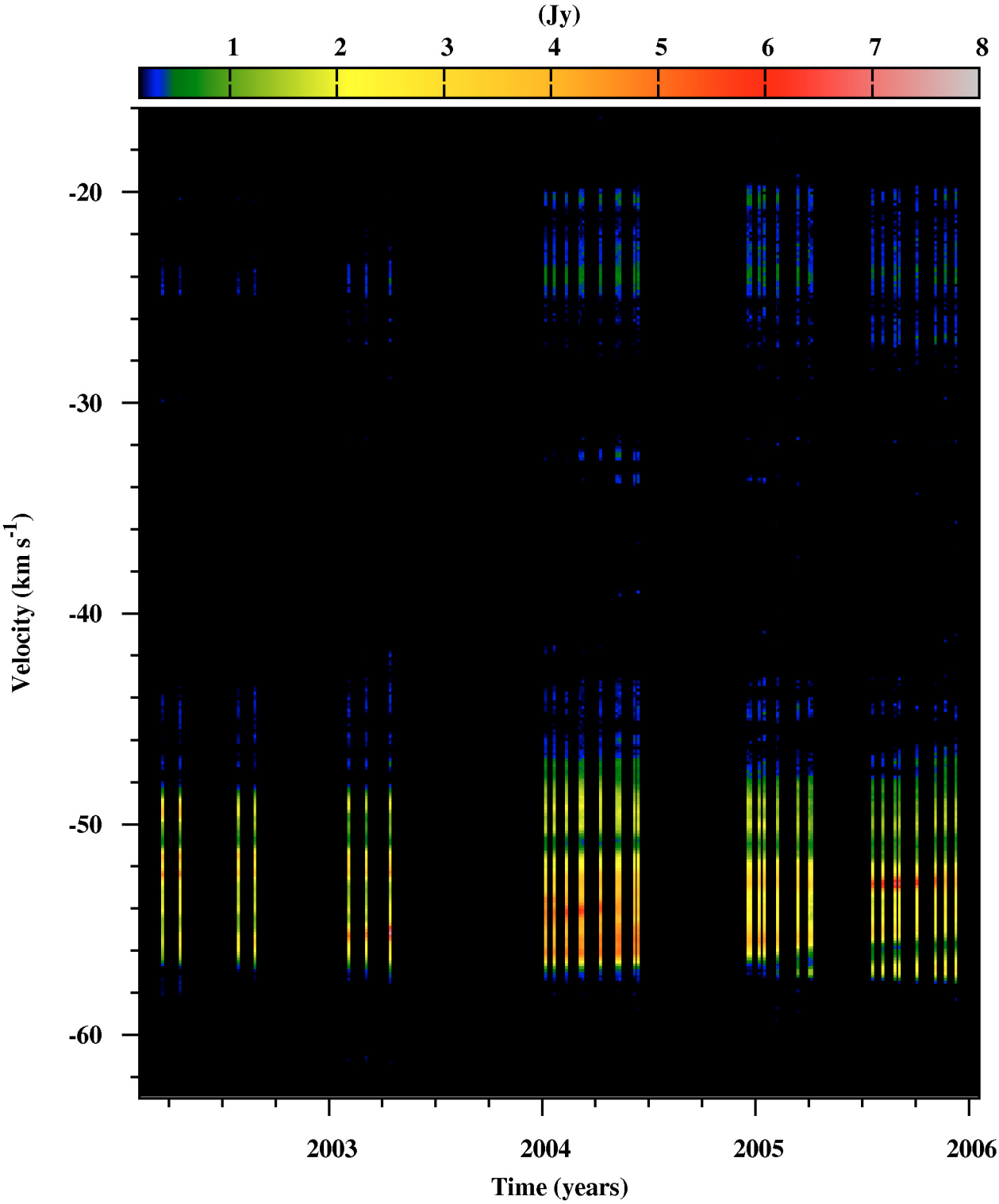

Fig. A.1. S Per 1667 MHz OH maser. The Stokes parameter *I* flux as a function of time and velocity.

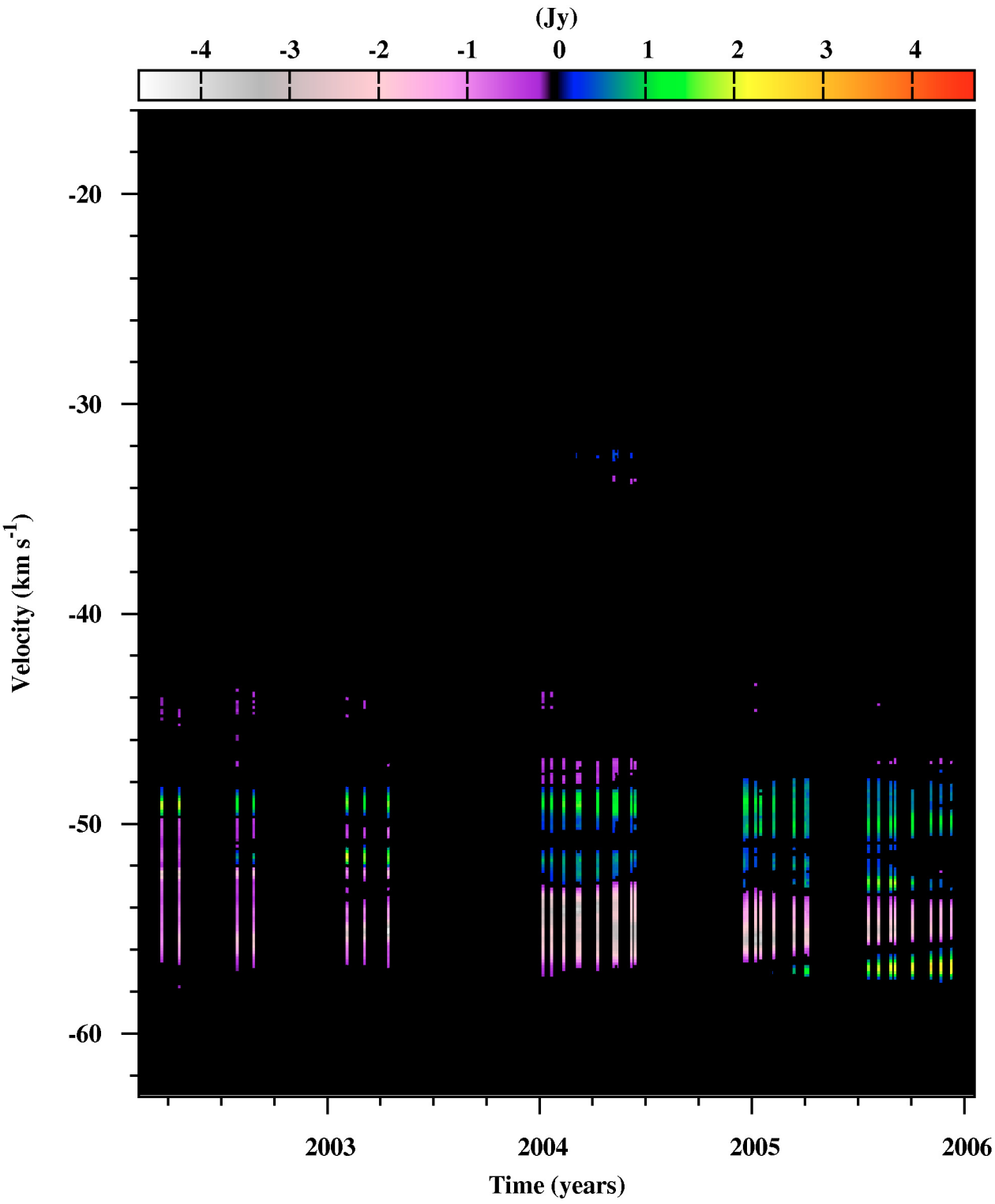

Fig. A.2. S Per 1667 MHz OH maser. The Stokes parameter *V* flux as a function of time and velocity.

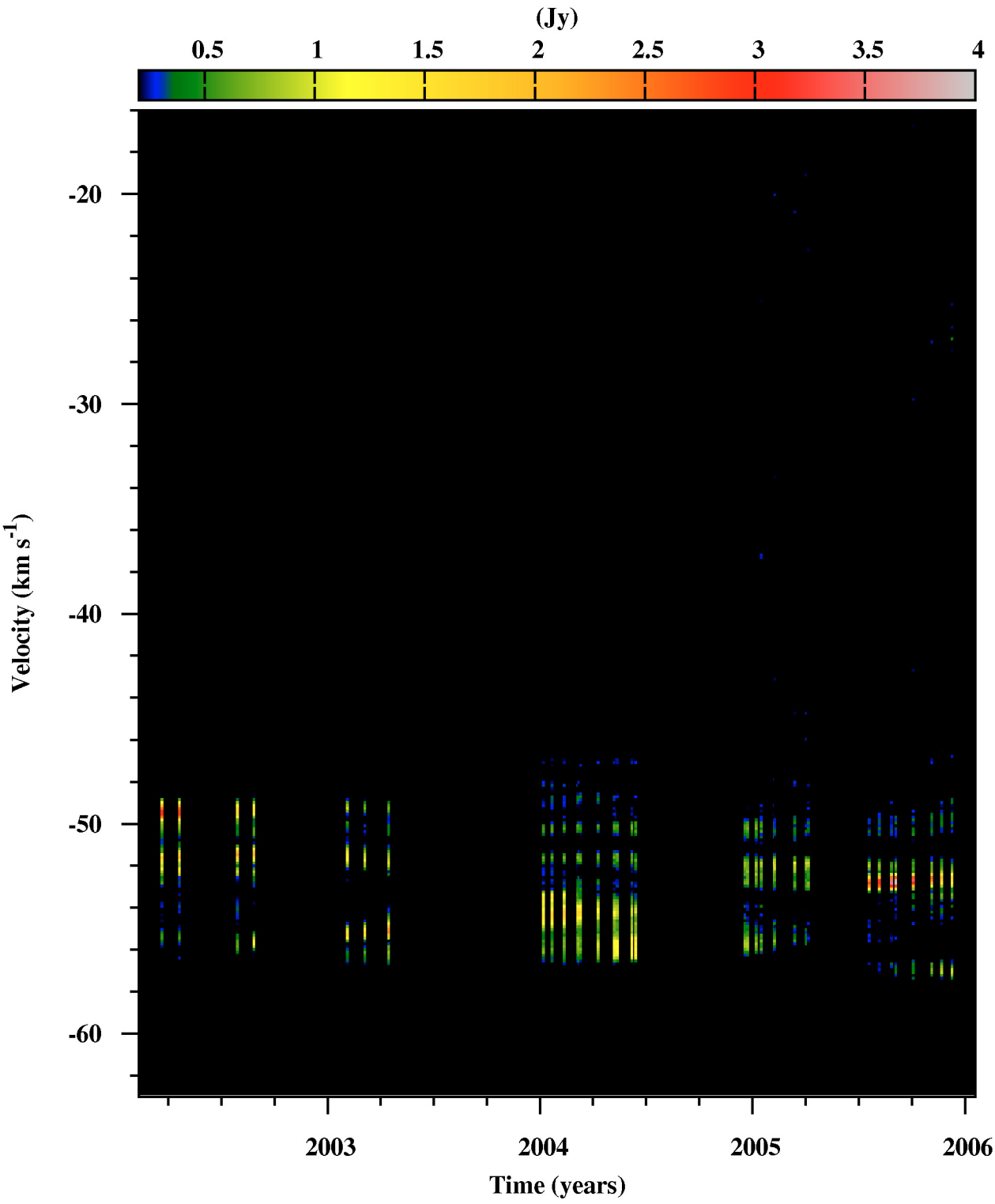

Fig. A.3. S Per 1667 MHz OH maser. The linearly polarized flux p as a function of time and velocity.

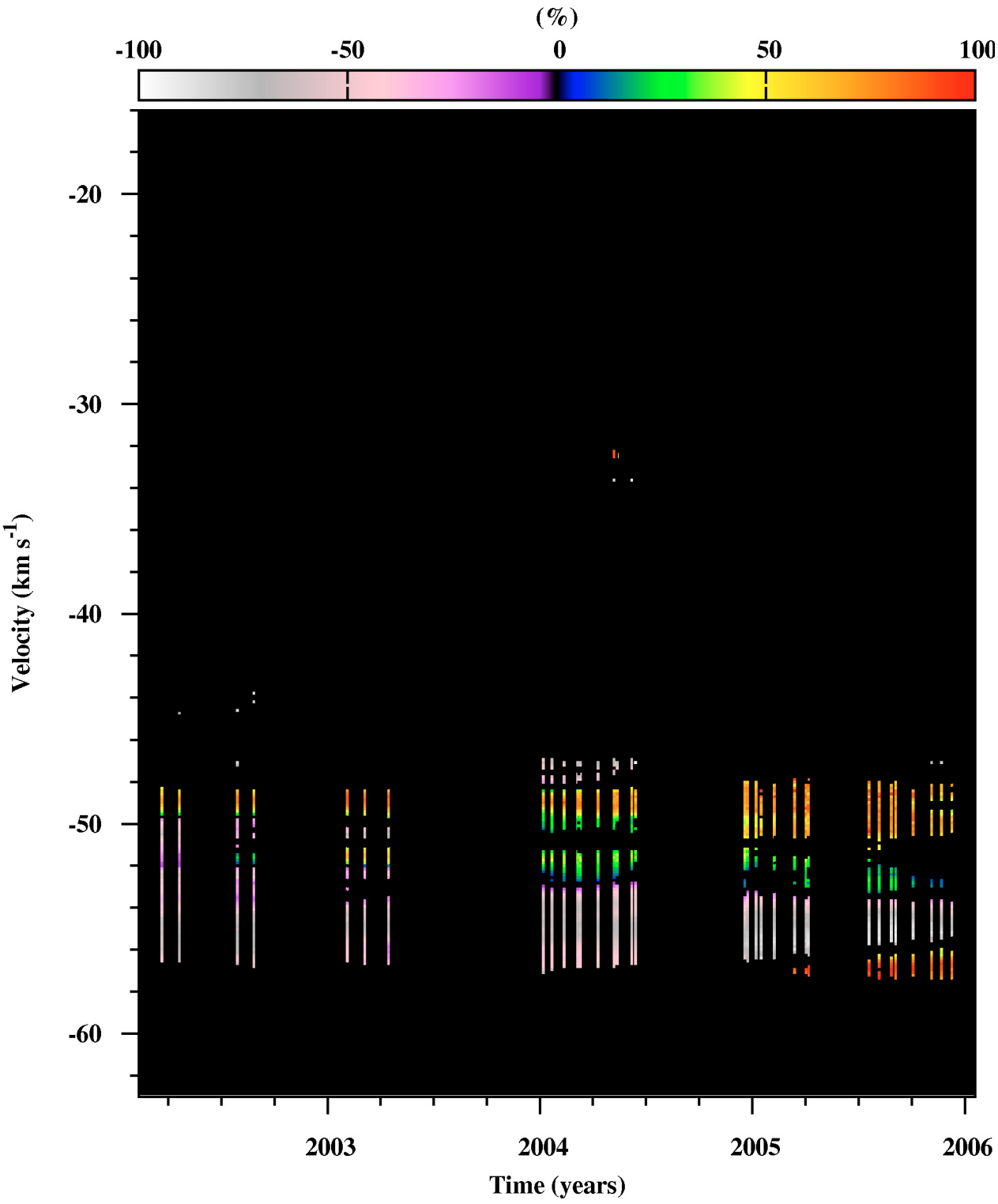

Fig. A.4. S Per 1667 MHz OH maser. The degree of circular polarization as a function of time and velocity.

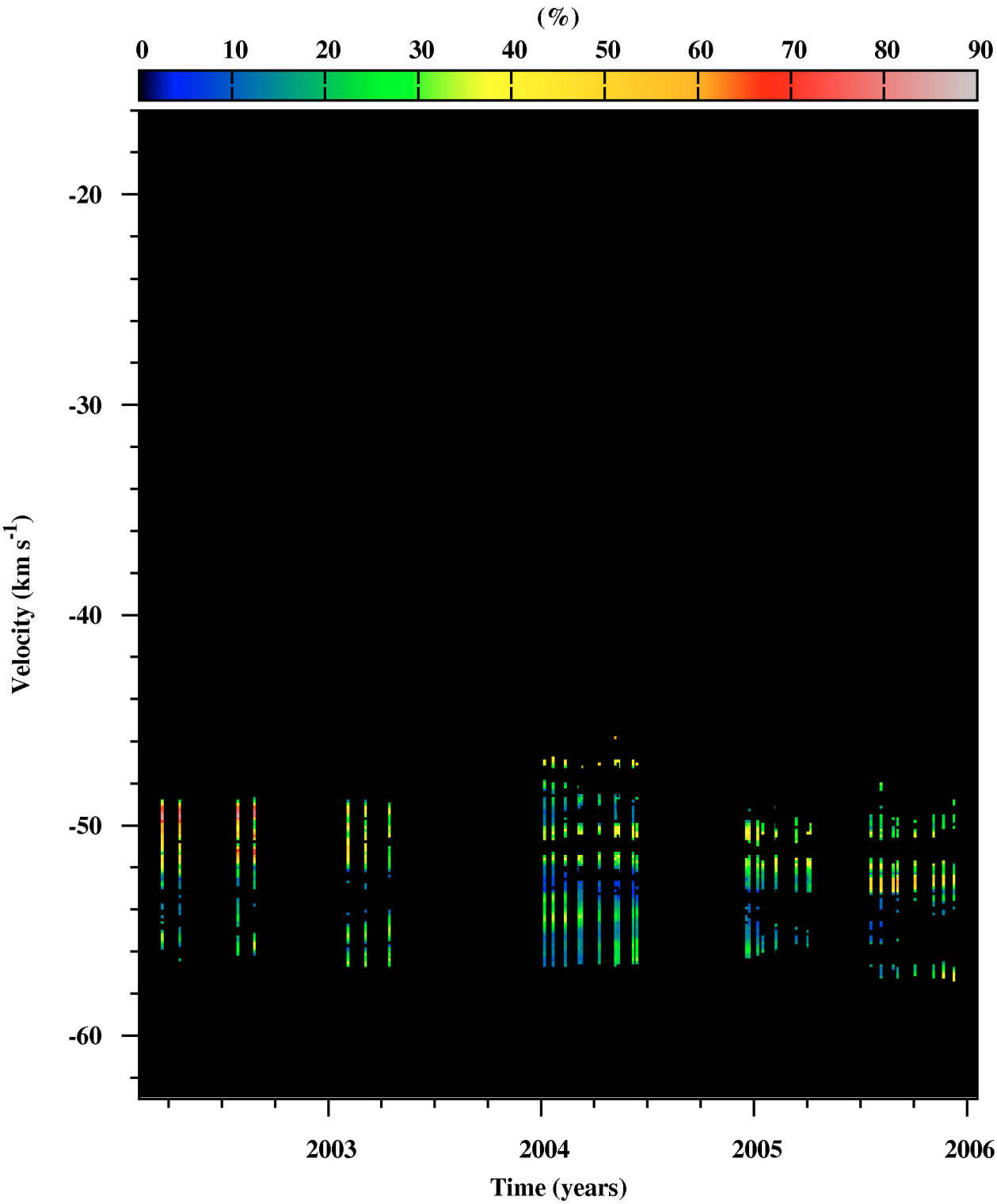

Fig. A.5. S Per 1667 MHz OH maser. The degree of linear polarization as a function of time and velocity.

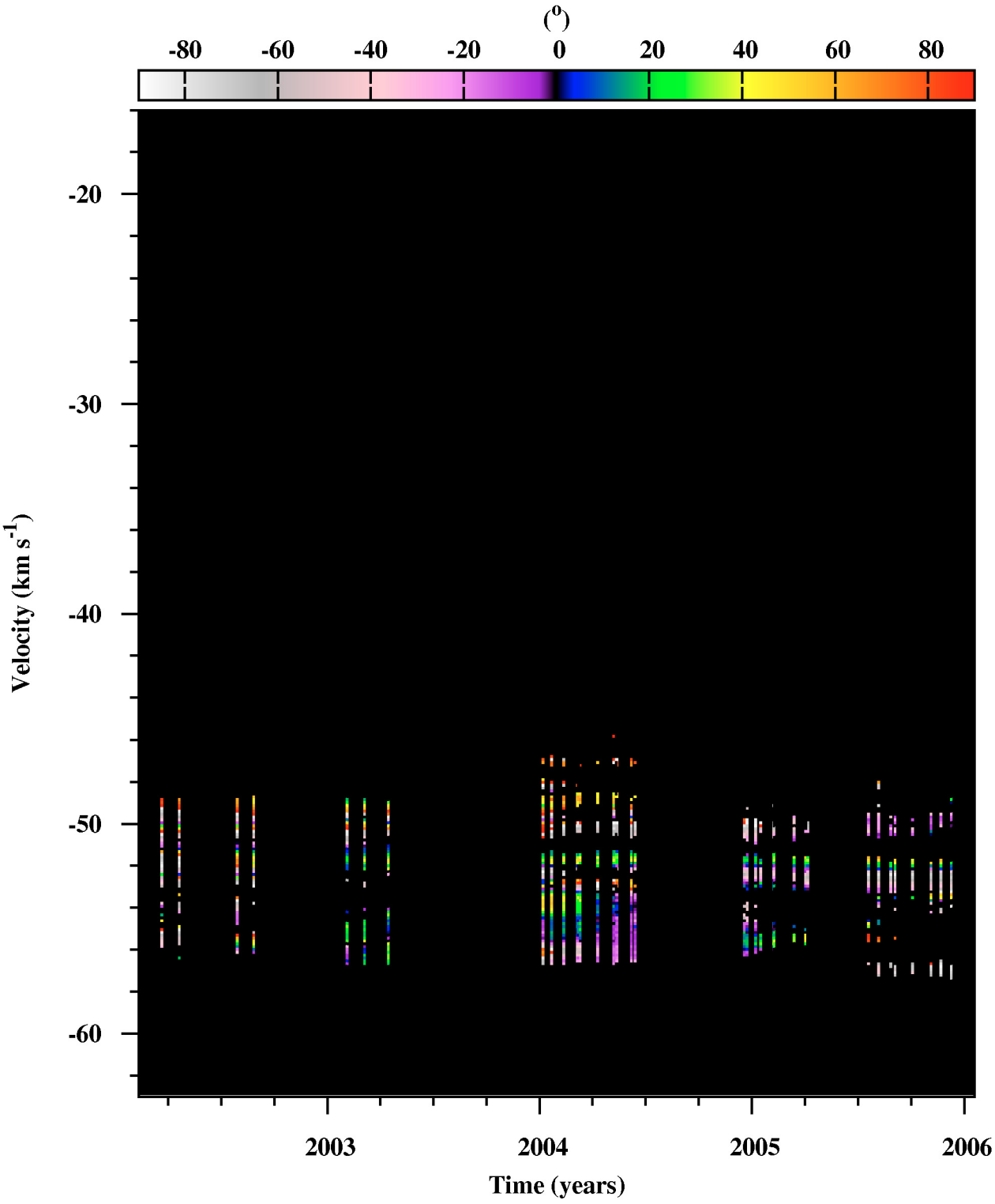

Fig. A.6. S Per 1667 MHz OH maser. The position angle of linear polarization as a function of time and velocity.

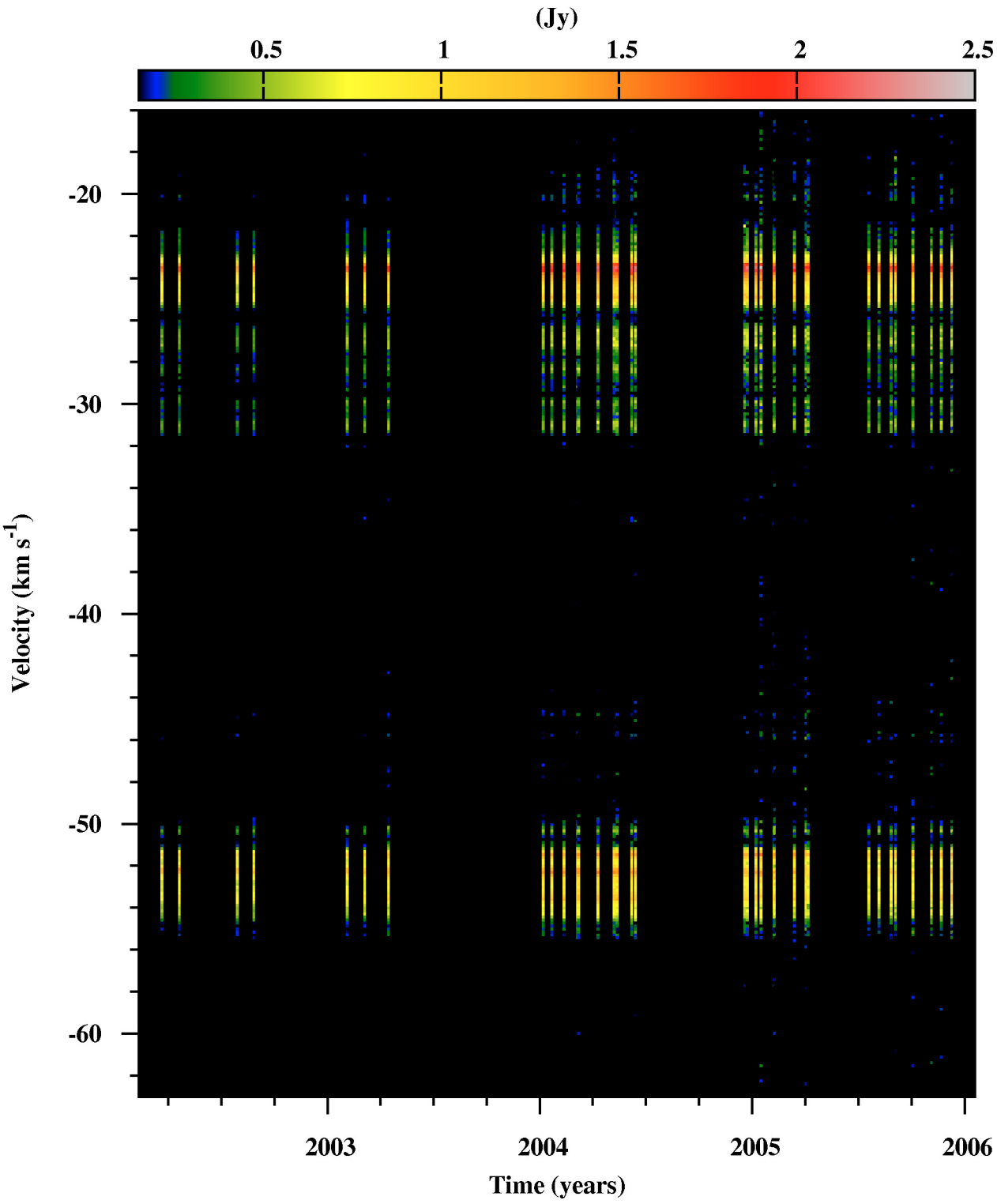

Fig. A.7. S Per 1612 MHz OH maser. The Stokes parameter *I* flux as a function of time and velocity.

Appendix B: Polarization spectra of VX Sgr at 1667 and 1612 MHz

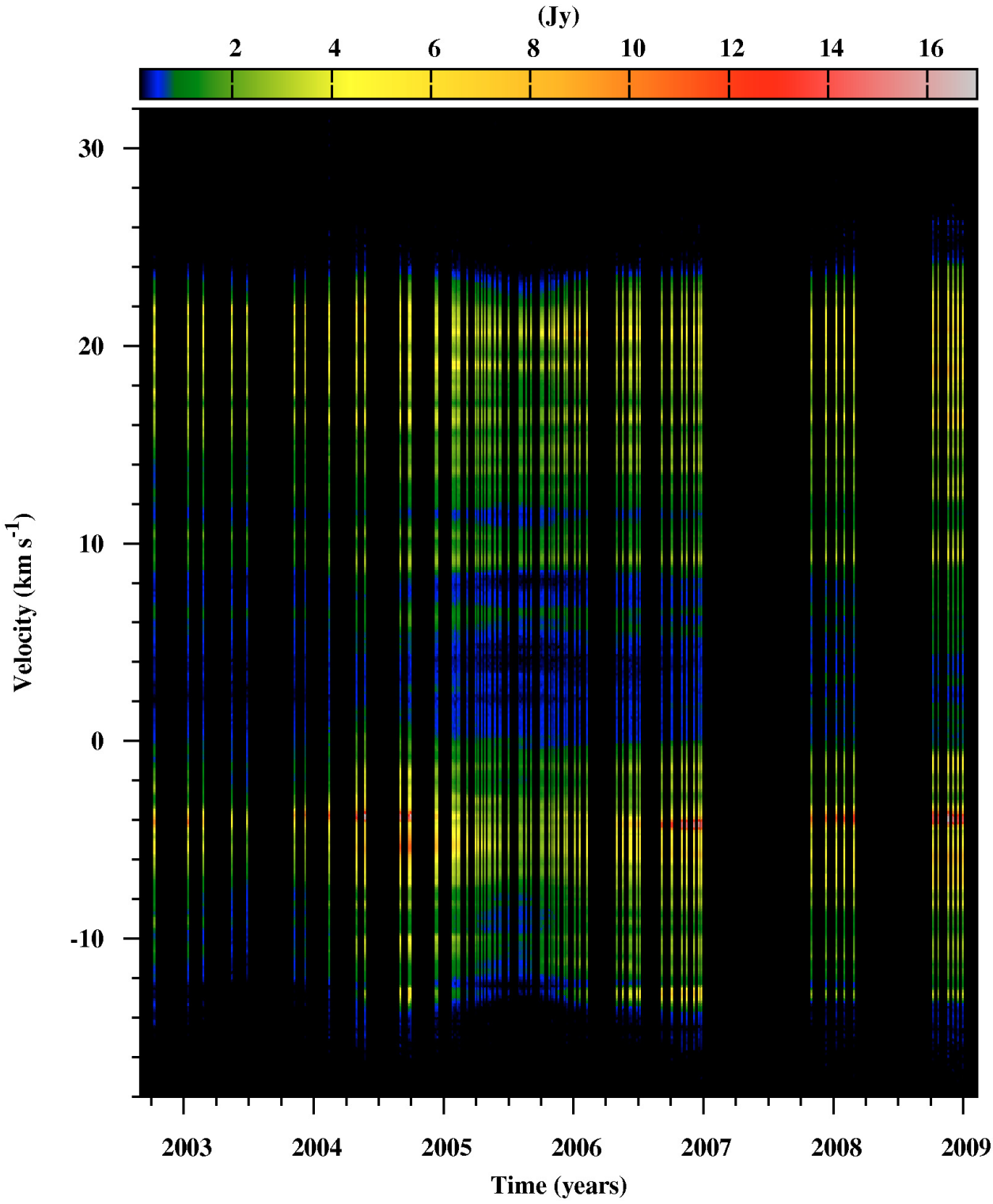

Fig. B.1. VX Sgr 1667 MHz OH maser. The Stokes parameter *I* flux as a function of time and velocity.

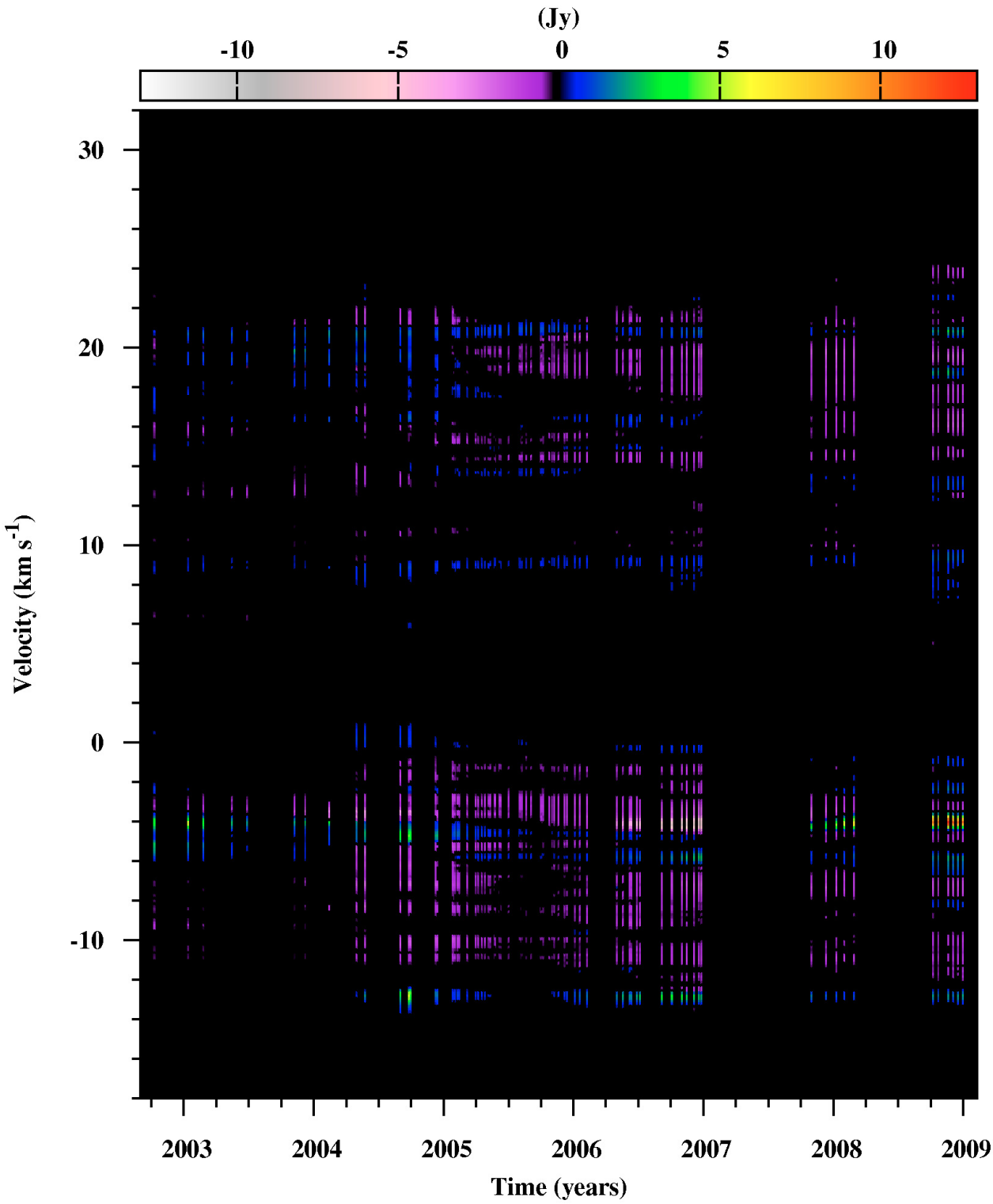

Fig. B.2. VX Sgr 1667 MHz OH maser. The Stokes parameter *V* flux as a function of time and velocity.

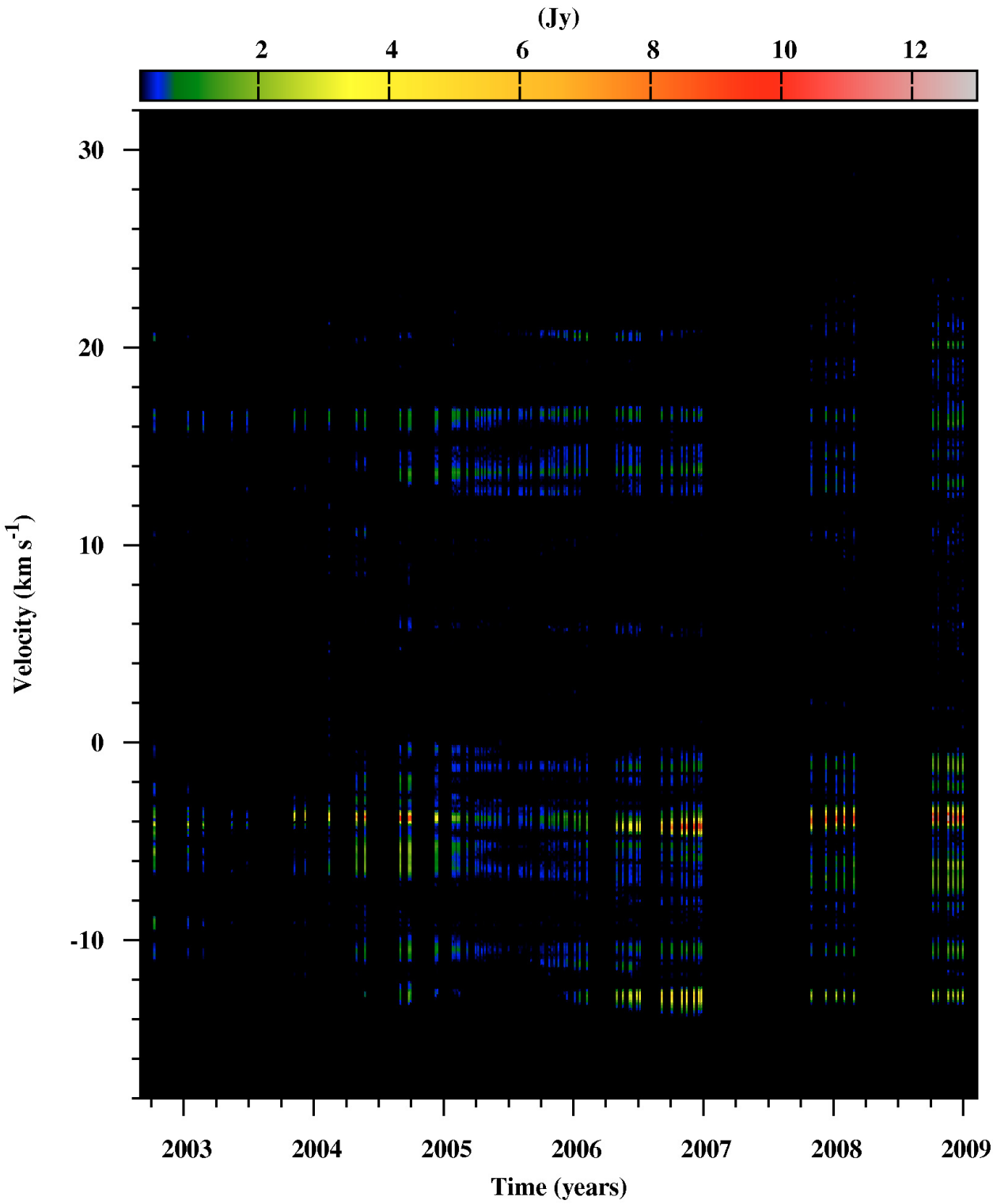

Fig. B.3. VX Sgr 1667 MHz OH maser. The linearly polarized flux p as a function of time and velocity.

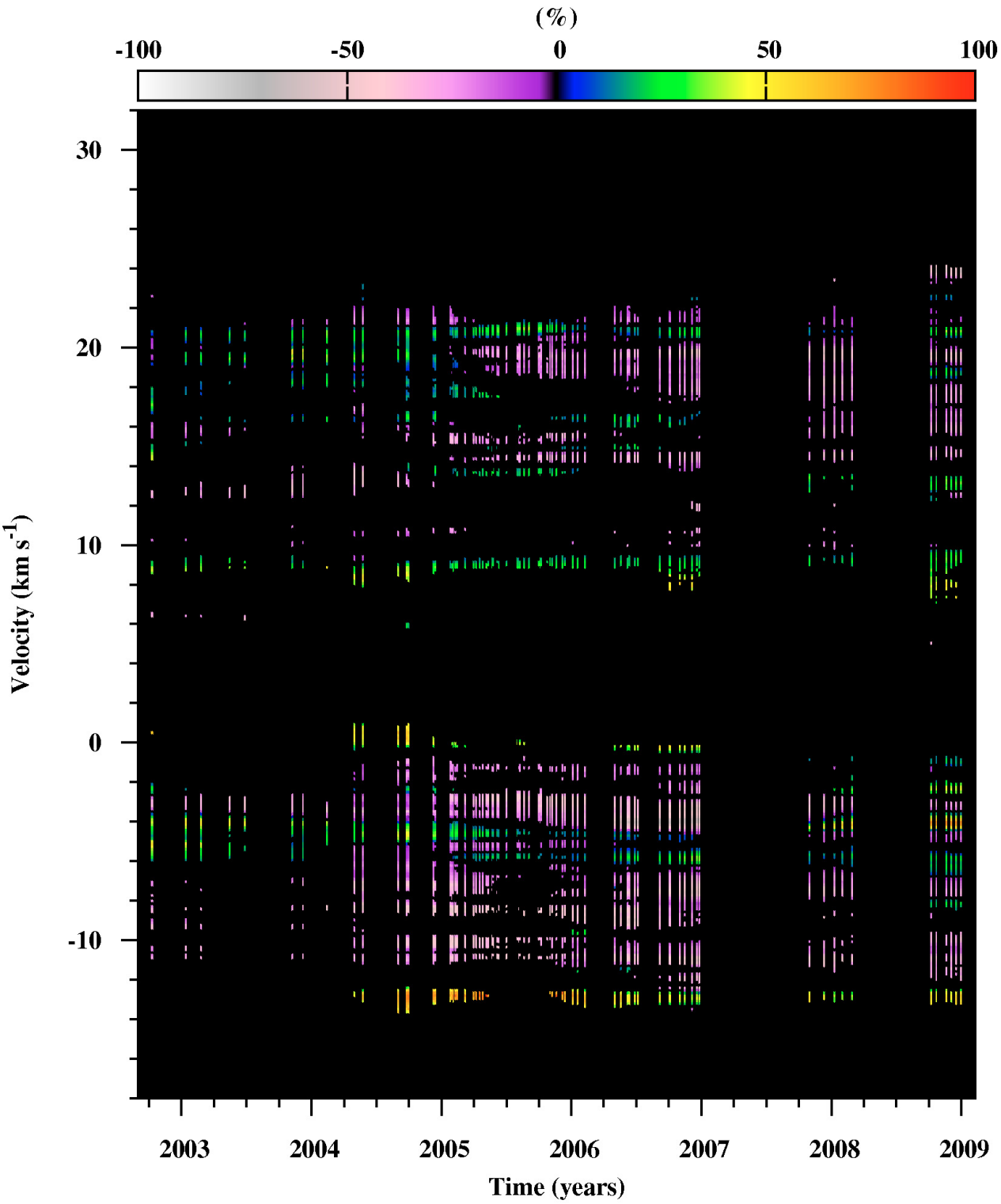

Fig. B.4. VX Sgr 1667 MHz OH maser. The degree of circular polarization as a function of time and velocity.

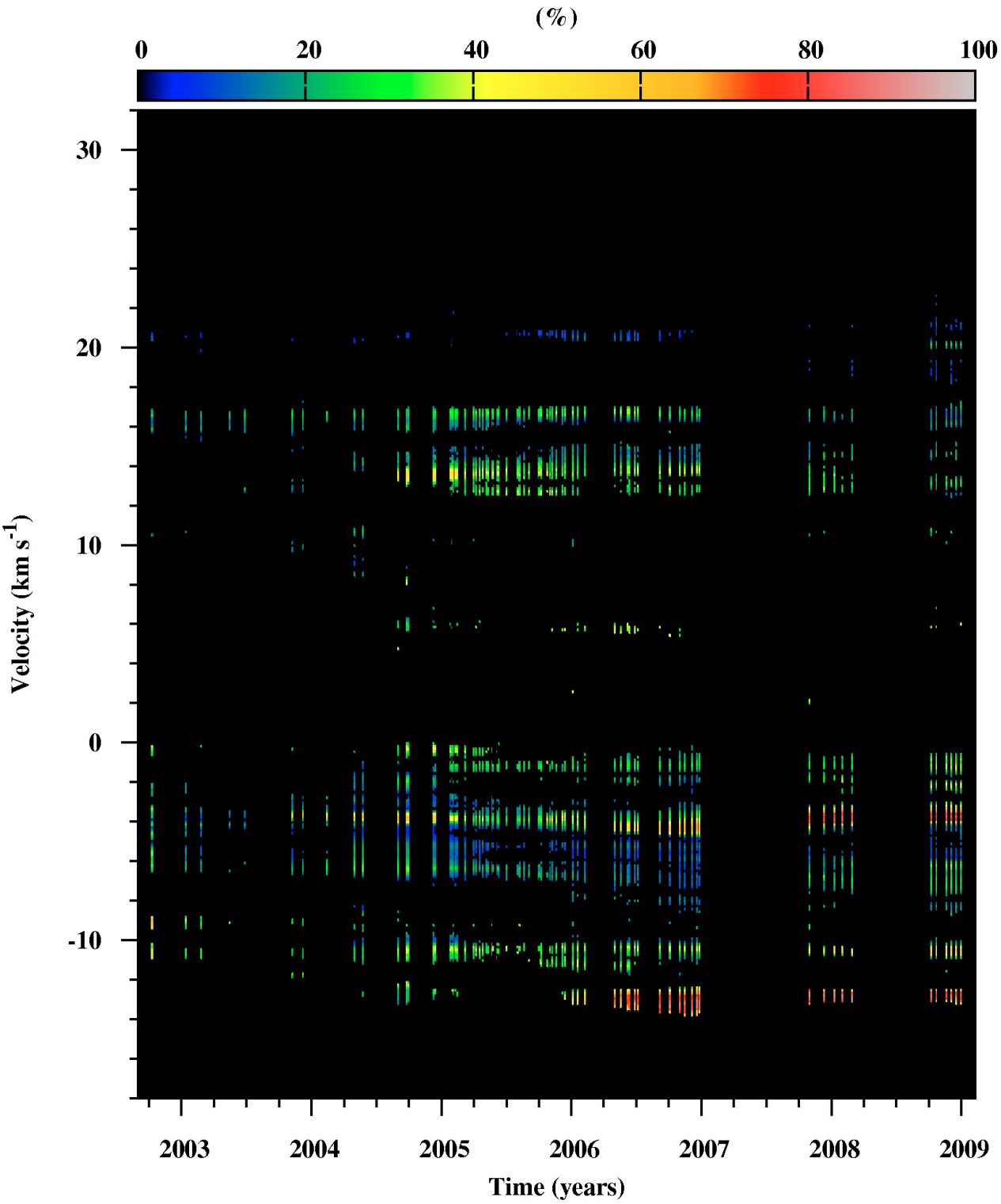

Fig. B.5. VX Sgr 1667 MHz OH maser. The degree of linear polarization as a function of time and velocity.

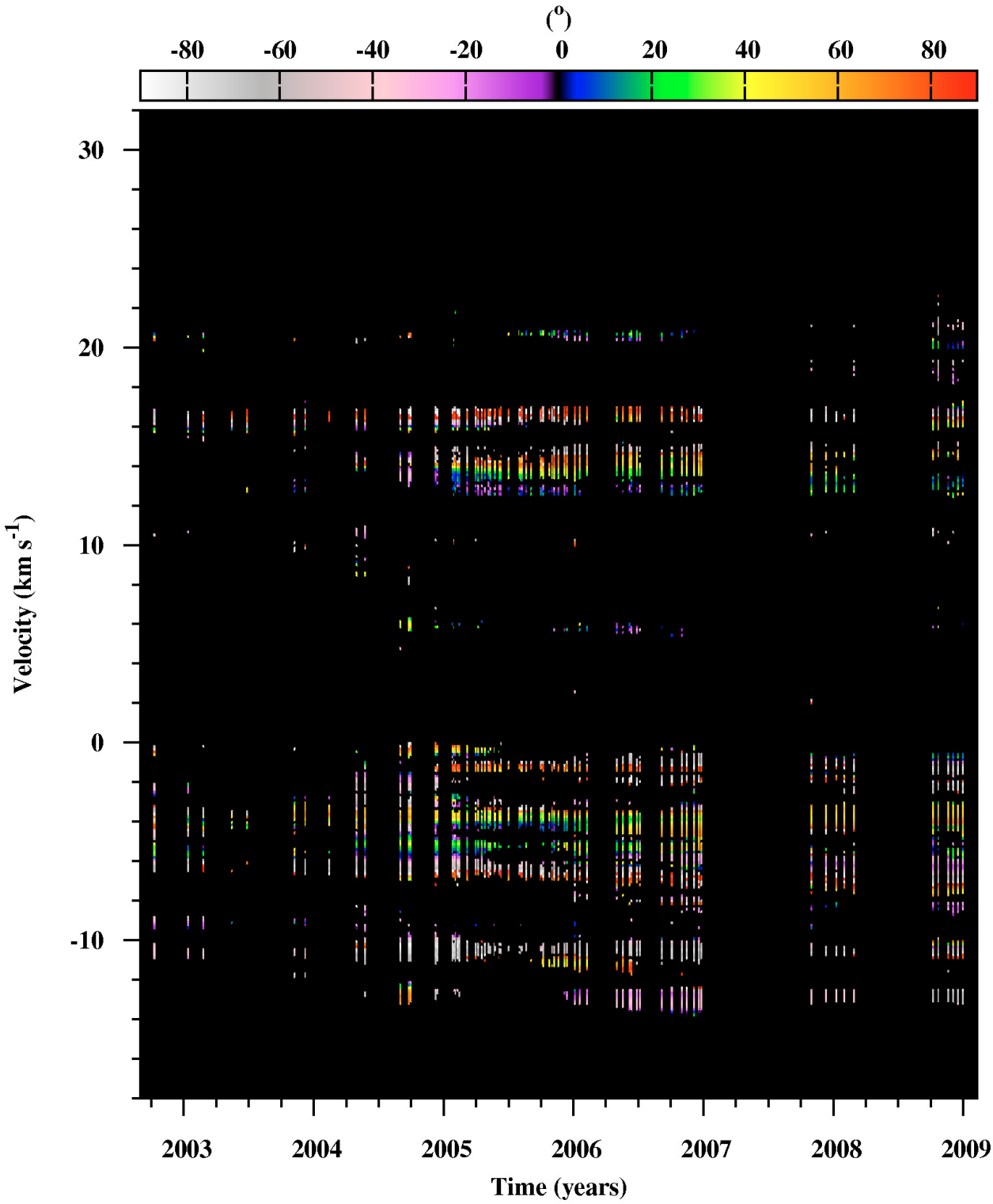

Fig. B.6. VX Sgr 1667 MHz OH maser. The position angle of linear polarization as a function of time and velocity (v <5.5 km s^{-1}).

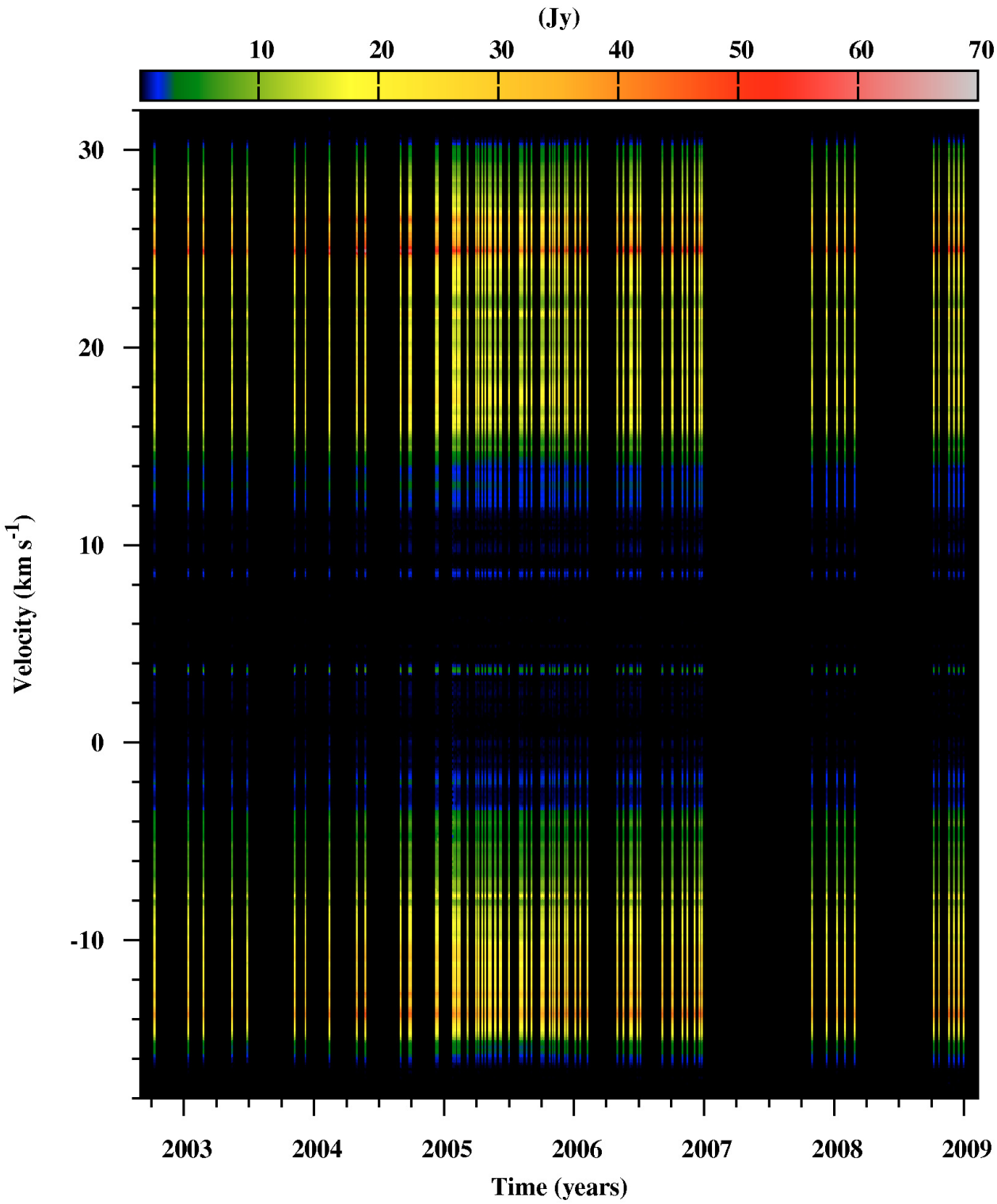

Fig. B.7. VX Sgr 1612 MHz OH maser. The Stokes parameter *I* flux as a function of time and velocity.

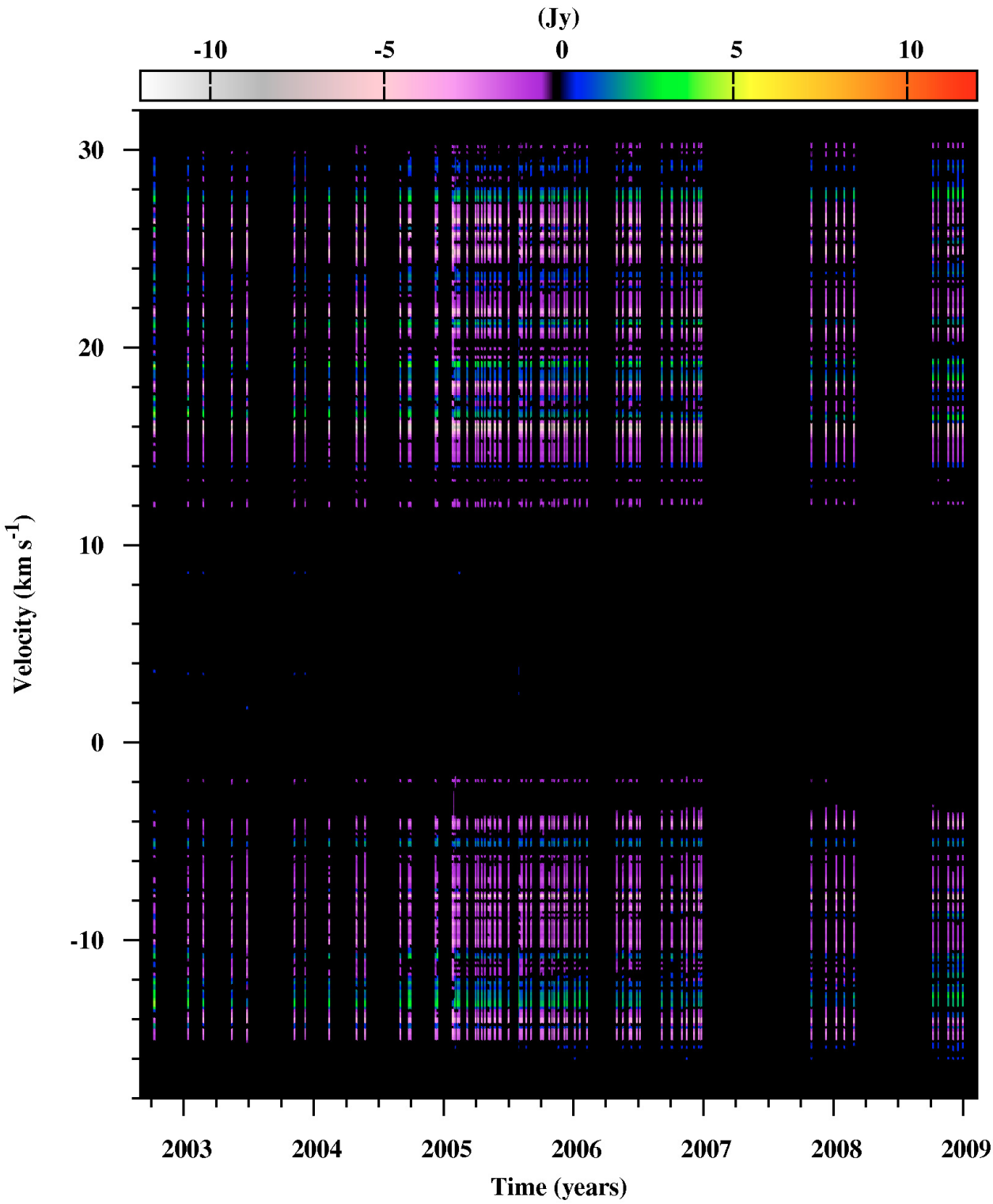

Fig. B.8. VX Sgr 1612 MHz OH maser. The Stokes parameter *V* flux as a function of time and velocity.

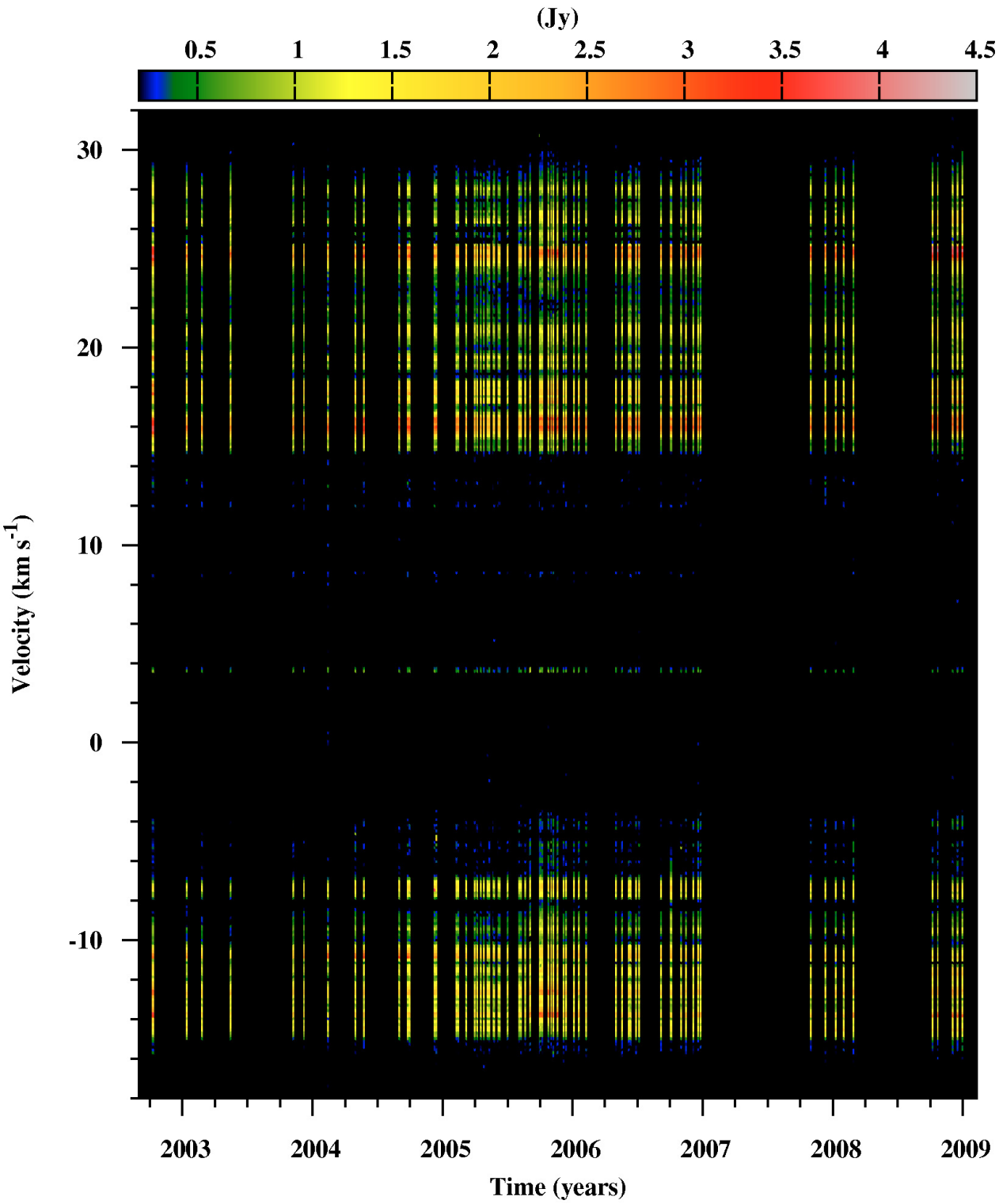

Fig. B.9. VX Sgr 1612 MHz OH maser. The Stokes parameter *p* flux as a function of time and velocity.

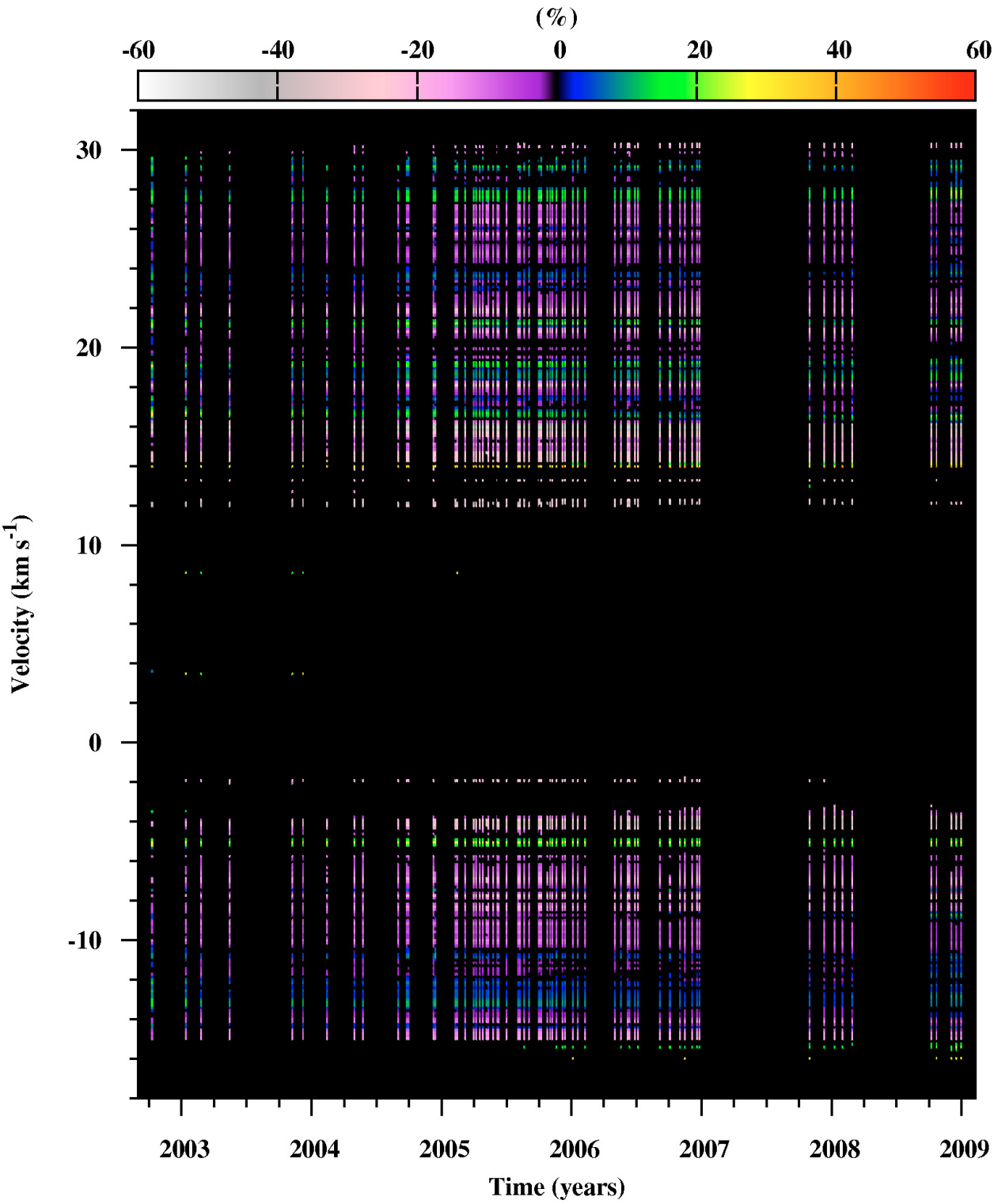

Fig. B.10. VX Sgr 1612 MHz OH maser. The degree of circular polarization as a function of time and velocity.

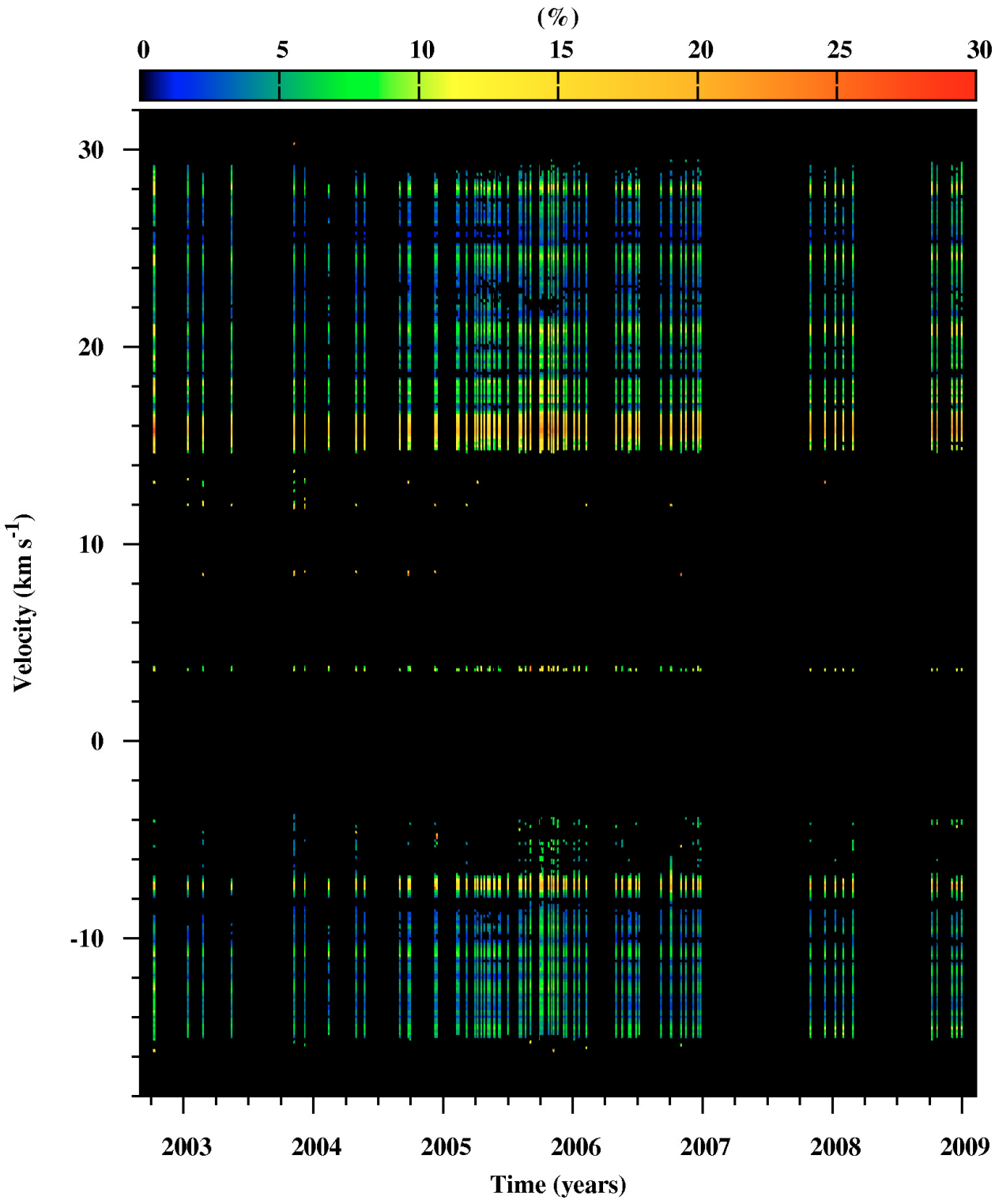

Fig. B.11. VX Sgr 1612 MHz OH maser. The degree of linear polarization as a function of time and velocity.

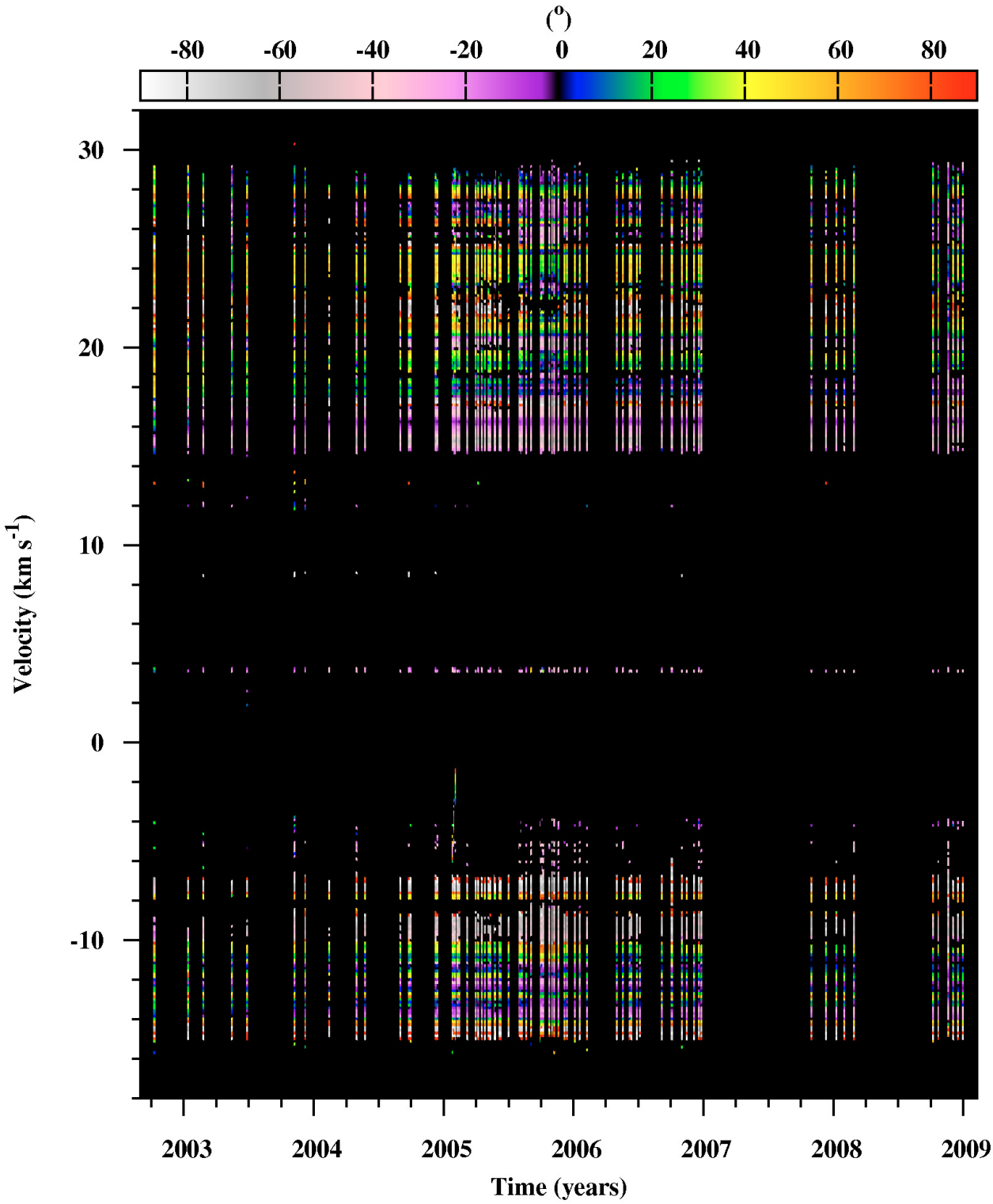

Fig. B.12. VX Sgr 1612 MHz OH maser. The position angle of linear polarization as a function of time and velocity.